Nowcasting Convective Activity for Space Shuttle Landings during Easterly Flow Regimes

WILLIAM H. BAUMAN III AND MICHAEL L. KAPLAN

Department of Marine, Earth and Atmospheric Sciences, North Carolina State University, Raleigh, North Carolina

STEVEN BUSINGER

Department of Meteorology, University of Hawaii at Manoa, Honolulu, Hawaii

(Manuscript received 10 January 1996, in final form 10 September 1996)

ABSTRACT

Space shuttle landings at the shuttle landing facility at Kennedy Space Center are subject to strict weather-related launch commit criteria and flight rules. Complex launch commit criteria and end-of-mission flight rules demand very accurate nowcasts (forecasts of less than 2 h) of cloud, wind, visibility, precipitation, turbulence, and thunderstorms prior to shuttle launches and landings.

During easterly flow regimes the onset of convective activity has proven to be particularly difficult to predict. Contrasting weather ranging from clear skies to thunderstorms occurs on days with seemingly similar synoptic environments. Four days of easterly flow during the Convection and Precipitation/Electrification (CaPE) Experiment were investigated in an effort to identify and simulate key features that distinguish convectively active and suppressed conditions. Data from CaPE and operational data, including satellite imagery and National Centers for Environmental Prediction model analysis output over the Florida peninsula and surrounding data-sparse Atlantic Ocean, are combined in the research. It is found that elevated moisture in the midtroposphere above the marine boundary layer helps distinguish convectively active and passive days. Moreover, analysis reveals that the moisture distribution is related to jet dynamics in the upper troposphere.

A series of simulations using the Mesoscale Atmospheric Simulation System (MASS) model was undertaken. The MASS model run with a coarse grid (45 km) correctly simulates the development of the upper-level jet streak and its general impact on convective activity over the Florida peninsula. The MASS model run with a nested (11 km) grid and moisture enhancement of the initial model state from radar, satellite, and surface data results in the best short-term (6 h) forecast of relative humidity and precipitation patterns over the Florida peninsula and proximate coastal environment. Implications of the research results for nowcasting convective activity over Cape Canaveral are discussed.

1. Introduction

Space shuttle launches and landings at the shuttle landing facility at Kennedy Space Center (KSC) are subject to strict weather-related launch commit criteria. Shuttle launches must accommodate the possibility of a shuttle emergency landing occurring between 25 and 105 min after launch (Bauman and Businger 1996).

Both modeling and observational studies have concluded that the patterns and locations of Florida convection are directly related to the synoptic wind field (Byers and Rodebush 1948; Estoque 1962; Frank et al. 1967; Neumann 1971; Pielke 1974; Boybeyi and Raman 1992). These studies demonstrate the importance of the interaction between the synoptic-scale wind and the sea-breeze circulation in determining the timing and locations of convective activity across the Florida peninsula. The sea-breeze circulation and the normal patterns of convection assume different characteristics depending on whether the prevailing low-level flow has an onshore, offshore, or alongshore component with respect to Florida's Atlantic coast (Arritt 1993).

Onshore (easterly) flow regimes along the Atlantic coast typically generate less vigorous convection than offshore (westerly) flow regimes (Foote 1991). Onshore flow conditions are characterized by a shallow low-level maritime moist layer, capped by a subsidence layer with dry conditions aloft. Onshore flow convection typically consists of small convective cloud towers that result in brief periods of showers. Blanchard and López (1985) presented south Florida rainfall patterns by synoptic characterization. For onshore flows, they discuss two different synoptic-type days. The first is characterized as a ''type-1 day'' with ''easterly flow'' and weak synoptic-scale forcing resulting in more dominant penin-

Corresponding author address: Dr. William H. Bauman III, Headquarters Air Weather Service, Technology, Plans, and Programs, 102 West Losey Street, Room 105, Scott AFB, IL 62225-5206.
E-mail: baumanw@hqaws.safb.af.mil

sular scale forcing. Further, the majority of the convection takes place in the sea-breeze and lake-breeze convergence zones. The second synoptic-type day is characterized as a ''type-2 day'' with stable lapse rates and low moisture values that discourage convection over the Florida peninsula. They also state that convection is sparse and requires a considerable amount of low-level forcing to set off convection. Generally, during onshore flow, only when the east coast sea breeze has moved to the west coast and has merged with the west coast sea breeze is there enough low-level forcing to generate deep convection. However, it is not a requirement for the two sea breezes to merge for convection to develop. Convection does develop independently of sea-breeze frontal merger, but it is usually weaker than when the fronts merge. Southwesterly flows tend to be more unstable and to produce more lightning strikes along the Florida east coast than easterly flow (Reap 1994). The southwesterly flow also contains deeper moisture and accounts for two-thirds of the lightning strikes during summer at KSC. In contrast, easterly flows account for less than 5% of the total lightning flashes (Watson et al. 1991).

Observations and model results show the sea breeze consists of two bands where convergence and upward vertical motions exist in the lower atmosphere (1–3 km) along each of Florida's coasts. Frank et al. (1967) and Burpee (1979) analyzed wind and radar observations over south Florida to describe sea-breeze behavior. The sea breeze fronts move inland depending on the large-scale lower- and midlevel circulation over the southeastern United States.

Pielke (1974) and Boybeyi and Raman (1992) used three-dimensional numerical models to investigate the behavior of the sea-breeze fronts over Florida. Their results show two areas of upward vertical motion in the boundary layer along each coast early in the model runs for both southeasterly and southwesterly ambient flow. Both of these areas are capable of producing (weak) convection. Under synoptic southeast flow, showers develop inland from both coasts with the eastern shower band moving westward during the day. By late afternoon, thunderstorms are present along the west coast with clear skies prevailing along the east coast. Both observations and model results suggest eastern Florida receives rainfall earlier on days with easterly flow than on days with westerly flow.

The Florida sea-breeze scenario does not sufficiently describe the varying conditions present with continued onshore flow. Low-level convergence and upward vertical motion present in the morning along a sea-breeze front over the east coast of Florida during onshore flow sometimes leads to the development of convection, but weather conditions can range from widespread thunderstorms to no precipitation. Since even a small onshore-moving shower or thunderstorm presents an unacceptable hazard to an orbiter trying to land at the shuttle landing facility (see Bauman and Businger 1996), this ambiguity presents a special forecast challenge in support of shuttle landings.

The primary objective of this research is to improve the lead time and accuracy of forecasts of the onset of convective activity at KSC during onshore flow regimes.

2. Analysis methodology

The research presented in this paper focuses on a series of days under easterly flow during the field phase of the Convection and Precipitation/Electrification (CaPE) Experiment. CaPE was a major field program conducted in central Florida from 8 July to 18 August 1991 (Foote 1991). CaPE investigations concentrated on the area encompassing KSC and Cape Canaveral Air Station (CCAS) in part to study weather impacts to the national space program. The CaPE field program resources included eight instrumented research aircraft, four Doppler radars, 47 Portable Automated Mesonet (PAM) surface stations, and six Cross-chain Loran Atmospheric Sounding Systems (CLASS; Fig. 1). The CaPE dataset was complemented by the KSC/CCAS observational network [wind tower mesonet, ground-based electric field mill network, and the lightning detection and ranging system; see Fig. 4 in Bauman and Businger (1996)] and routinely available operational data (hourly surface observations, twice-daily rawinsondes, buoys, ships of opportunity, and satellite data).

Easterly flow generally prevails across the Florida peninsula in the summer when the western ridge of the Bermuda high lies through central and northern Florida (Pielke 1975). However, during CaPE the prevailing flow was westerly, with only 9 days classified as easterly. Of these 9 days, 4, 19–22 July, were contiguous with most CaPE instrumentation up and running providing good observational coverage and are the focus of this research. On 19 and 20 July, the prevailing flow was east to southeasterly, while on 21 and 22 July the prevailing flow was more easterly. These 4 days are somewhat synoptically similar to the Blanchard and Lopez (1985) type-1 and type-2 days discussed in section 1 of this paper but they do not fit the type-1 finding that states weak synoptic-scale forcing results in more dominant peninsular-scale forcing. On the days that most closely represent a type-1 day, there is little peninsular-scale forcing, as will be shown later in this paper. Also, the findings in this paper reflect data from these four days which is not intended to represent a climatological study of this forecast problem.

The only conventional data over water during the period of investigation were from occasional ships of opportunity and two buoys (Fig. 1), which reported at synoptic times. Overwater analyses were constructed by merging actual rawinsonde data with ''synthetic'' soundings derived from the National Centers for Environmental Prediction (NCEP) Nested Grid Model (NGM) analyses (National Oceanic and Atmospheric Administration 1985). The NCEP Global Optimum In-

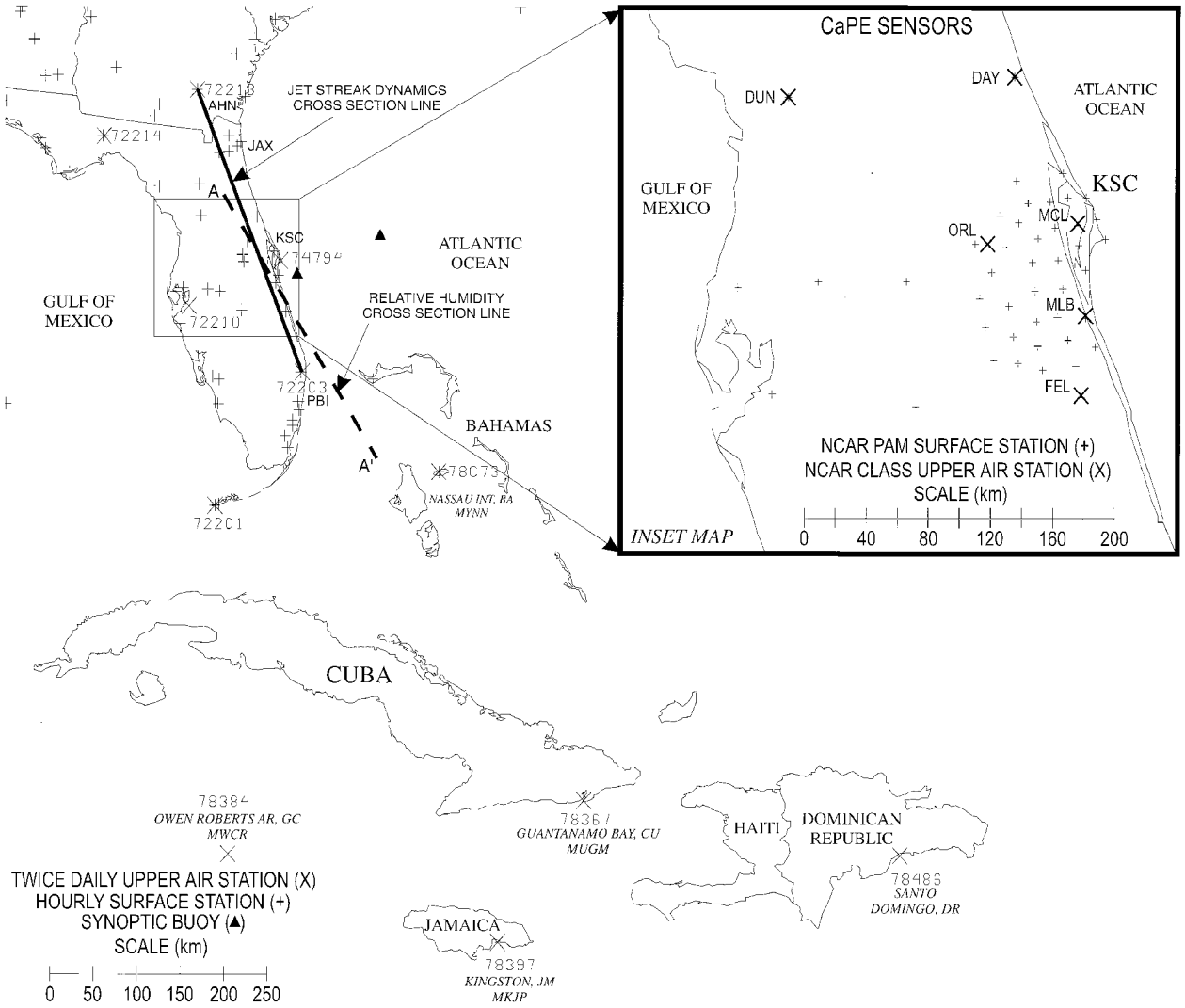

FIG. 1. Map of Florida and the northern Caribbean region showing locations of the hourly surface observing stations (+) and the twice daily rawinsonde release sites (×). The solid line from AHN to PBI gives the location of the cross sections in Fig. 6, whereas the dashed line labeled A to A′ gives the location of vertical cross sections shown in Fig. 8. The inset map shows the locations of the special CaPE sensors: the PAM surface observing systems (+) and the CLASS release sites (×).

terpolation (GOI) spectral analysis was used as a ''first guess'' field for the merged rawinsonde and NGM sounding data (Table 1). The General Meteorological Package (GEMPAK; desJardins et al. 1992) was then used to create a sounding at each NGM and GOI grid point. The NGM soundings were merged with actual CLASS, National Weather Service, and U.S. Air Force rawinsondes. The GOI sounding analyses were gridded at 0.5° × 0.5° horizontal grid spacing (56 km × 56 km) and used as the first-guess field for a Barnes objective analysis (Barnes 1973) performed on the merged NGM and rawinsonde sounding data. The resulting GEMPAK data arrays, which combined all available data in a 40 km × 40 km grid, were used for all the mesoscale analyses in this research.

3. Active, passive, and suppressed days

a. Definitions

In order to define the relative amount of convective activity, each day was classified into one of three different categories: active, passive, or suppressed. As the terms suggest, on an active day convection was observed to be widespread across the KSC area, on a passive day the convection was present but somewhat less than an active day, and on a suppressed day there was little or no convection present.

b. Observed satellite imagery

On 19 July, convective showers are seen in the KSC area (Fig. 2a). These showers moved northwest and were

TABLE 1. Vertical levels in the Nested Grid Model (NGM) archive dataset and Global Optimum Interpolation (GOI) archive dataset. NGM-archived fields include geopotential height (Φ), temperature (*T*), relative humidity (RH), and *u* and *v* components. GOI-archived fields include mean sea level pressure (MSLP), temperature (*T*), and sea surface temperature (SST) at the surface and geopotential height (Φ), temperature (*T*), and *u* and *v* components of wind at all other levels. The GOI-archived fields also include RH from the surface through 300 mb.

Pressure level (mb)	NGM archive grid	GOI archive grid
Surface		MSLP, *T*, SST
1000	Φ, *T*, RH, *u*, *v*	Φ, *T*, RH, *u*, *v*
950	Φ, *T*, RH, *u*, *v*	
900	Φ, *T*, RH, *u*, *v*	
850	Φ, *T*, RH, *u*, *v*	Φ, *T*, RH, *u*, *v*
800	Φ, *T*, RH, *u*, *v*	
750	Φ, *T*, RH, *u*, *v*	
700	Φ, *T*, RH, *u*, *v*	Φ, *T*, RH, *u*, *v*
500	Φ, *T*, RH, *u*, *v*	Φ, *T*, RH, *u*, *v*
300	Φ, *T*, RH, *u*, *v*	Φ, *T*, RH, *u*, *v*
250		Φ, *T*, *u*, *v*
200		Φ, *T*, *u*, *v*
150		Φ, *T*, *u*, *v*

over KSC from about 1400 until 1700 UTC. By 1800 UTC an east coast sea-breeze front had developed and was moving westward toward central Florida, leaving the east coast of the peninsula clear. This day is classified as an ''active'' convective day at KSC.

The most active of the 4 days was 20 July (Fig. 2b) with bands of convective showers moving onshore throughout the morning. Showers were occurring at KSC by 1200 UTC and moved out of the area by about 1700 UTC. Waterspouts were observed offshore from KSC and Patrick Air Force Base (45 km south of KSC) between 1200 and 1300 UTC. The convection that had moved onshore in the morning slowly merged with a developing east coast sea-breeze front, which helped advect the showers northwestward away from KSC.

Convection was generally suppressed (passive) on 21 July (Fig. 2c). One convective shower developed offshore from Patrick Air Force Base, produced a waterspout from 1245 until 1300 UTC, dissipated shortly thereafter as it moved across Patrick Air Force Base, and convection was suppressed for the rest of the day. Convection on 22 July (Fig. 2d) was suppressed all day in the KSC vicinity. Showers and thunderstorms developed during the day inland over south Florida.

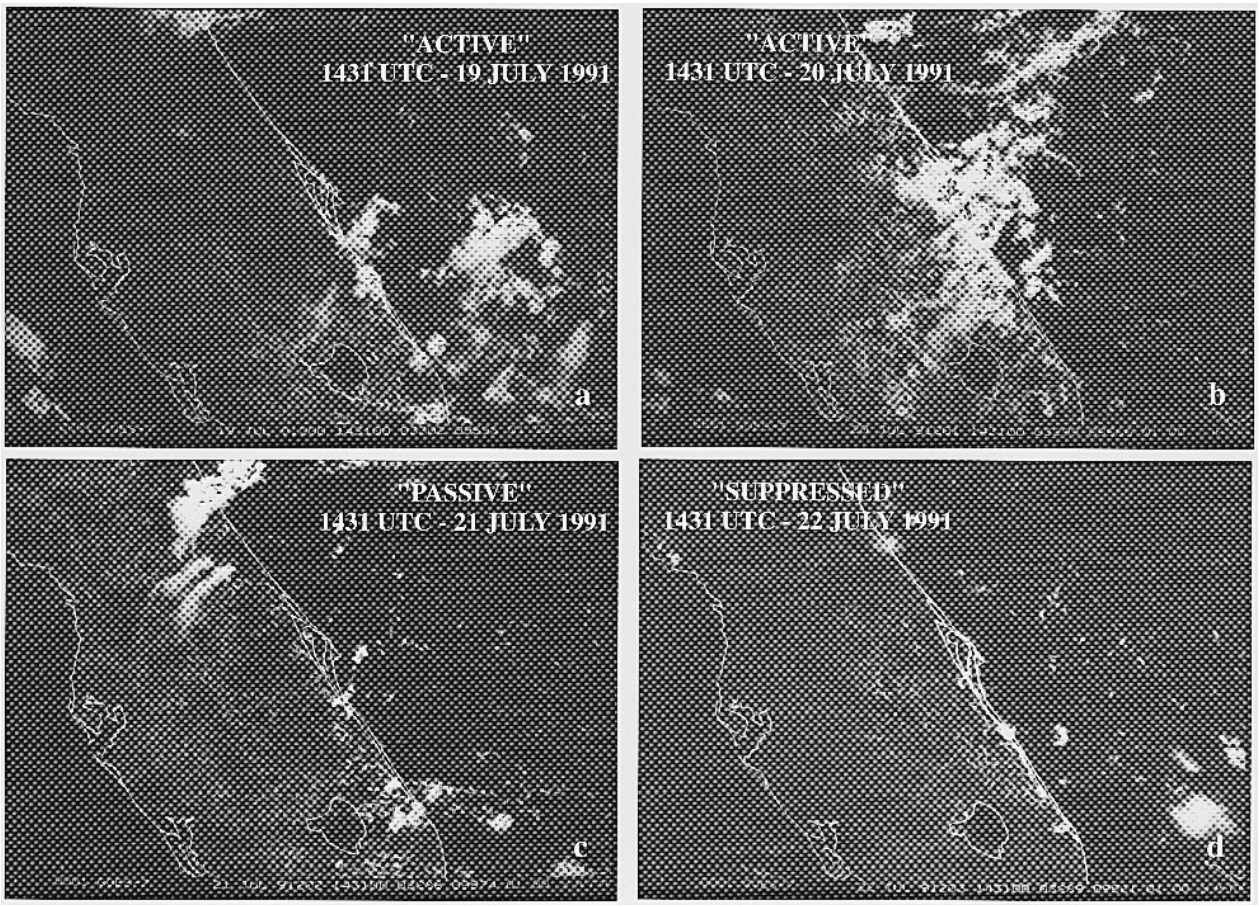

FIG. 2. Visible satellite imagery (1-km horizontal resolution) from *GOES-7* for (a) 1431 UTC 19 July 1991, (b) 1431 UTC 20 July 1991, (c) 1431 UTC 21 July 1991, and (d) 1431 UTC 22 July 1991. Location of KSC indicated.

TABLE 2. A timeline of the forecast and observed weather at KSC prepared by U.S. Air Force forecasters for 19–22 July 1991. The period in which precipitation was forecast is shown by the solid lines beginning and ending with a triangle. The type of precipitation forecast is written below each solid line. The actual time when convection occurred is shown by the dashed line beginning and ending with an open circle.

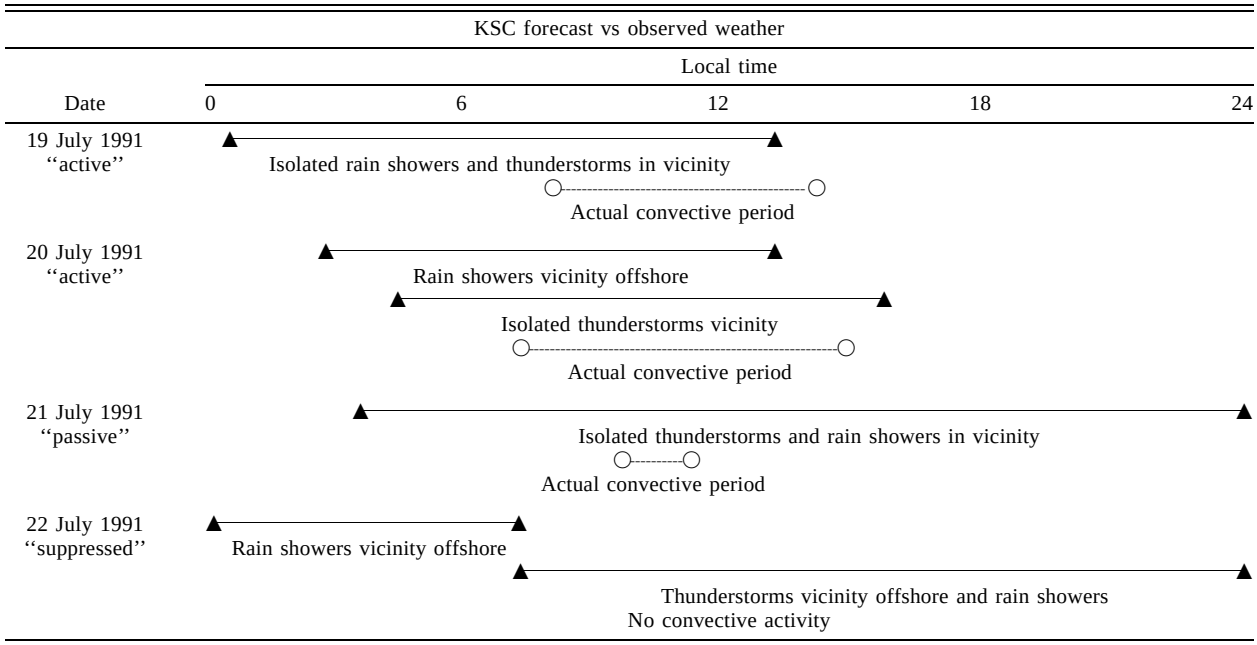

c. *Forecast difficulty*

The terminal forecasts for KSC, shown in Table 2, demonstrate the difficulty of forecasting convective activity during onshore flow. The weather at KSC was significantly different during the 4 days considered, but the terminal area forecasts issued by U.S. Air Force Range Weather Operations forecasters each morning varied little from day to day.

The terminal forecasts for the same 4 days issued by the Melbourne National Weather Service (Table 3) and the actual weather observed at Melbourne were consistent with the Range Weather Operations forecasts and KSC observations. It is clear that the forecasts changed little each day and the forecast matched the observed convective periods well on 19 and 20 July (the ''active'' days). However, on 21 July (a ''passive'' day) a few weak showers moved onshore and were in the KSC vicinity for less than 2 h, yet the forecast called for isolated thunderstorms and rain showers in the KSC vicinity from 0400 to 2400 local time (UTC − 4 h). On 22 July (a ''suppressed'' day) east-central Florida was devoid of convection, yet the KSC forecast called for early morning rain showers offshore from KSC with a change to rain showers at KSC and thunderstorms offshore from the KSC vicinity from 0900 to 2400 local time.

d. *Data analysis*

The surface analyses are typical for summer with a ridge of the Bermuda high extending westward to the southeast United States (Fig. 3). Surface pressures rise up to 4 mb over the southeast United States between 19 and 20 July as the surface ridge builds westward. Beyond 20 July at 1200 UTC (Fig. 3b), surface pressures remain fairly constant as the ridge becomes quasi-stationary. Without close scrutiny, the surface pattern appears ''similar'' on all 4 days, especially over east-central Florida. But closer inspection reveals the surface winds in east Florida are very light with a prevailing easterly component yet show a tendency to shift from southeast early in the period to northeast by the end. The slight change in wind direction is a subtle hint of a total column mass adjustment. Although the surface ridge does not build significantly after 1200 UTC 20 July (Fig. 3b), it does become closed with a weak circulation by 1200 UTC 21 July (Fig. 3c). This is an indication of subsidence and weak low-level divergence, which extends southward to central Florida.

The 850-mb analyses (not shown) and 700-mb analyses (Fig. 4) show high geopotential heights over the southwestern North Atlantic and southeastern United States with anticyclonic curvature over Florida. The ridge is located across central Florida at 1200 UTC 19 July (Fig. 4a) and slowly migrates northward until a closed high develops by 1200 UTC 21 July over Georgia (Fig. 4c). The high migrates west and is located over Alabama by 1200 UTC 22 July (Fig. 4d). Heights rise an average of 40 m over the southeast United States throughout the period. The building high at 850 and 700 mb is consistent with a developing area of low-level difluence over the southeast United States, helping to

TABLE 3. A timeline of forecast and observed weather at Melbourne, FL, prepared by National Weather Service forecasters for 19–22 July 1991. The period in which precipitation was forecast is shown by the solid lines beginning and ending with a triangle. The type of precipitation forecast is written below each solid line. The actual time when convection occurred is shown by the dashed line beginning and ending with an open circle.

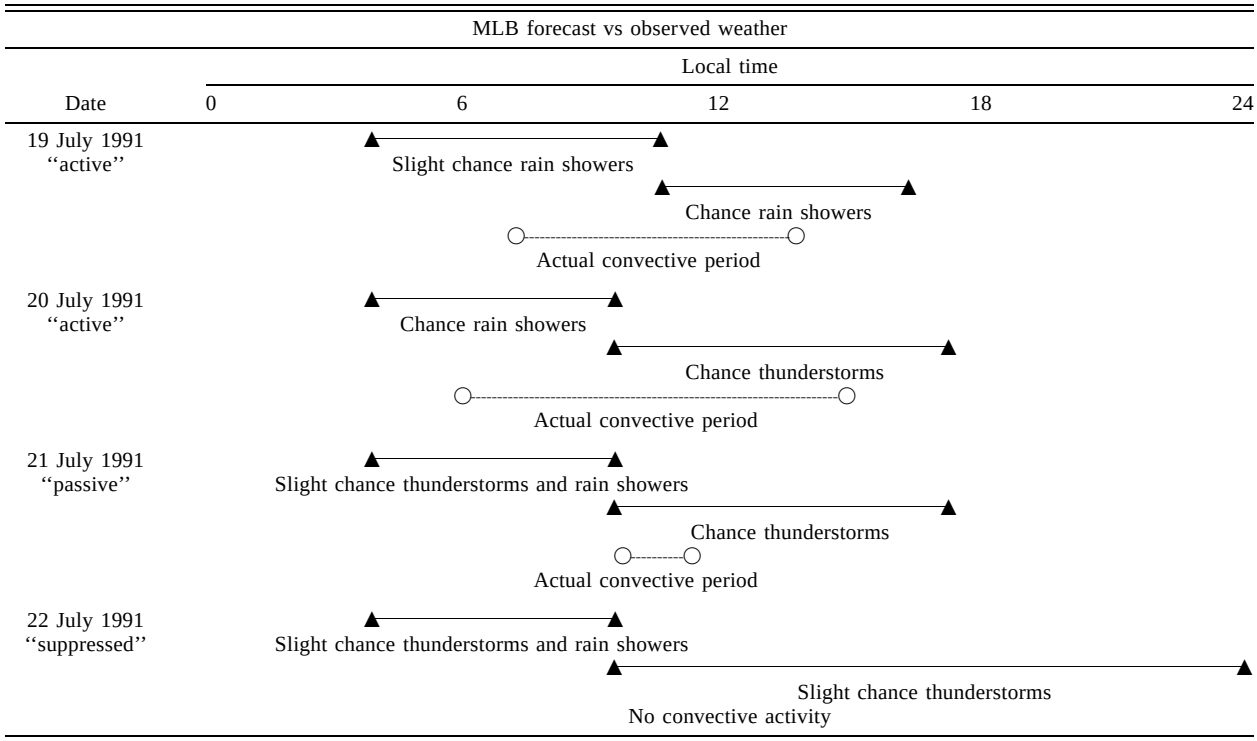

suppress convection later in the period over east-central Florida.

Analyses at the 150-mb level (Fig. 5) show a trough dominating the southwestern North Atlantic Ocean and Caribbean region through the period. A cold-core tropical upper-tropospheric trough (TUTT) is normally present over the subtropical and tropical Atlantic region in summer (Whitfield and Lyons 1992; Fitzpatrick et al. 1995). The long-term mean position of the TUTT axis at 200 mb during July is oriented east–west just south of Florida over Cuba and across the Yucatan Peninsula.

A closed low moved westward from east of the Bahamas at 1200 UTC 19 July (Fig. 5a) to just south of Florida by 1200 UTC 22 July (Fig. 5d). To reveal the 150-mb cold low in a summer subtropical environment, it was necessary to analyze height contours every 20 m and the isotachs every 5 m s^{-1}, instead of the conventional 120 m and 10 m s^{-1} intervals, respectively. Propagation of the cold low during the period tightens the height gradient over Florida and Georgia on 21 and 22 July, creating a jet streak of 20 m s^{-1} by 1200 UTC 22 July (Fig. 5d). A climatological study by Fitzpatrick et al. (1995) shows that closed circulations called cold lows or TUTT cells form within the tropical upper-tropospheric trough and move south and west along the TUTT axis throughout the summer.

The transverse circulations observed with the developing jet streak in this case are consistent with those of the jet-streak model (Uccellini and Johnson 1979; Kocin and Uccellini 1990). In the jet-streak model convection is enhanced in the left (south) exit region of the jet where upper-level positive vorticity advection and divergence are occurring and convection is suppressed in the left (south) entrance region of the jet where upper-level negative vorticity advection and convergence are occurring.

On 19 and 20 July, the flow over central Florida is weak and difluent (Figs. 5a and 5b). At this time, the jet streak is still off the east coast of Florida and is not evident in the analyses due to lack of observations over the water. However, based on the position of the jet streak and the cold low on the following 2 days (Figs. 5c and 5d), it can be assumed that the exit region of the jet streak is affecting Florida weather by 20 July (the most convectively active). On 21 July, the jet streak is centered over east-central Florida, indicating a transition from left (south) exit region to left entrance region in the KSC vicinity, consistent with the occurrence of weak convection early in the morning changing to more suppressed conditions later in the morning. Finally, on 22 July, the jet streak has moved north and west, leaving the KSC area under the influence of the left entrance region of the jet streak with upper-level convergence and downward vertical motion indirectly suppressing convection.

Vertical cross sections constructed orthogonal to the jet streak are shown in Fig. 6. The active day (20 July)

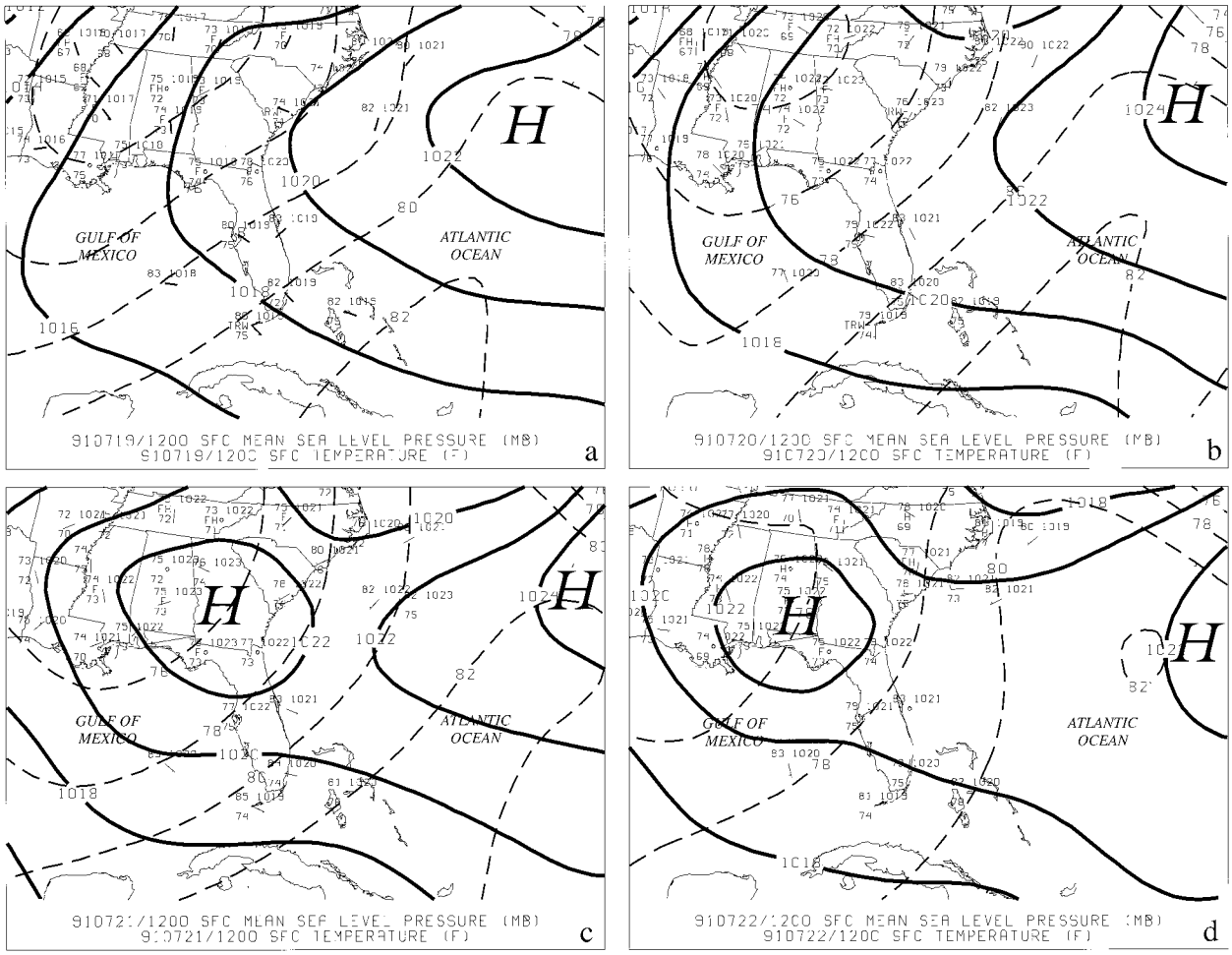

FIG. 3. Surface analyses of sea level pressure (solid contours every 2 mb) and temperature (dashed contours every 2°F) for (a) 1200 UTC 19 July 1991, (b) 1200 UTC 20 July 1991, (c) 1200 UTC 21 July 1991, and (d) 1200 UTC 22 July 1991. Surface observations are plotted with the usual convention with temperatures given in °F and winds where a half (full) barb equals 5 m s^{-1} (10 m s^{-1}).

at KSC (Fig. 6a) shows a benign pattern with near-zero vertical velocities throughout the domain and a region of 10 m s^{-1} winds (coming out of the page) from 250 to 150 mb. The jet streak is not evident at this time (Fig. 5b) since it is developing to the east of Florida in a data-sparse area. Widespread convection in the KSC vicinity on 20 July is consistent with the left (south) exit region of the jet contributing to destabilization. On 22 July (Fig 6b), the jet streak is north of Jacksonville (JAX) centered at about 150 mb. The jet entrance region is now affecting Florida with KSC beneath the left (south) entrance region resulting in upper-tropospheric convergence and downward vertical motion over this region. The transverse circulation shows leftward-directed motion across the jet entrance region and downward vertical motion (in agreement with the conceptual model), consistent with suppressed convection at this time. When the jet and its associated transverse circulations are simulated with the Mesoscale Atmospheric Simulation System (MASS) model at high resolution (discussed in section 4), the resulting robust circulations agree with satellite data and are consistent with the weaker dynamics found in the lower-resolution observational analysis presented here.

The first morning soundings at CCAS are released daily at ~1015 UTC (0615 LT) and are representative of the preconvective environment and background state in the KSC vicinity on days with onshore flow and morning shower activity. Morning soundings for 20 and 22 July (Fig. 7) reveal a contrast between the environments of the active and suppressed days. Deep easterlies were present each day with mostly weak southeasterly flow from the surface through 730 mb on 20 July (Fig. 7a), while the southeasterlies were confined to levels below 850 mb on 22 July (Fig. 7b). The temperature profiles are similar with slightly colder temperatures aloft (620–340 mb) on the active day, 20 July (Fig. 7a). The 500-mb temperatures were about 3°C colder on both active days than passive and suppressed days, providing a slightly more unstable environment during the first 2

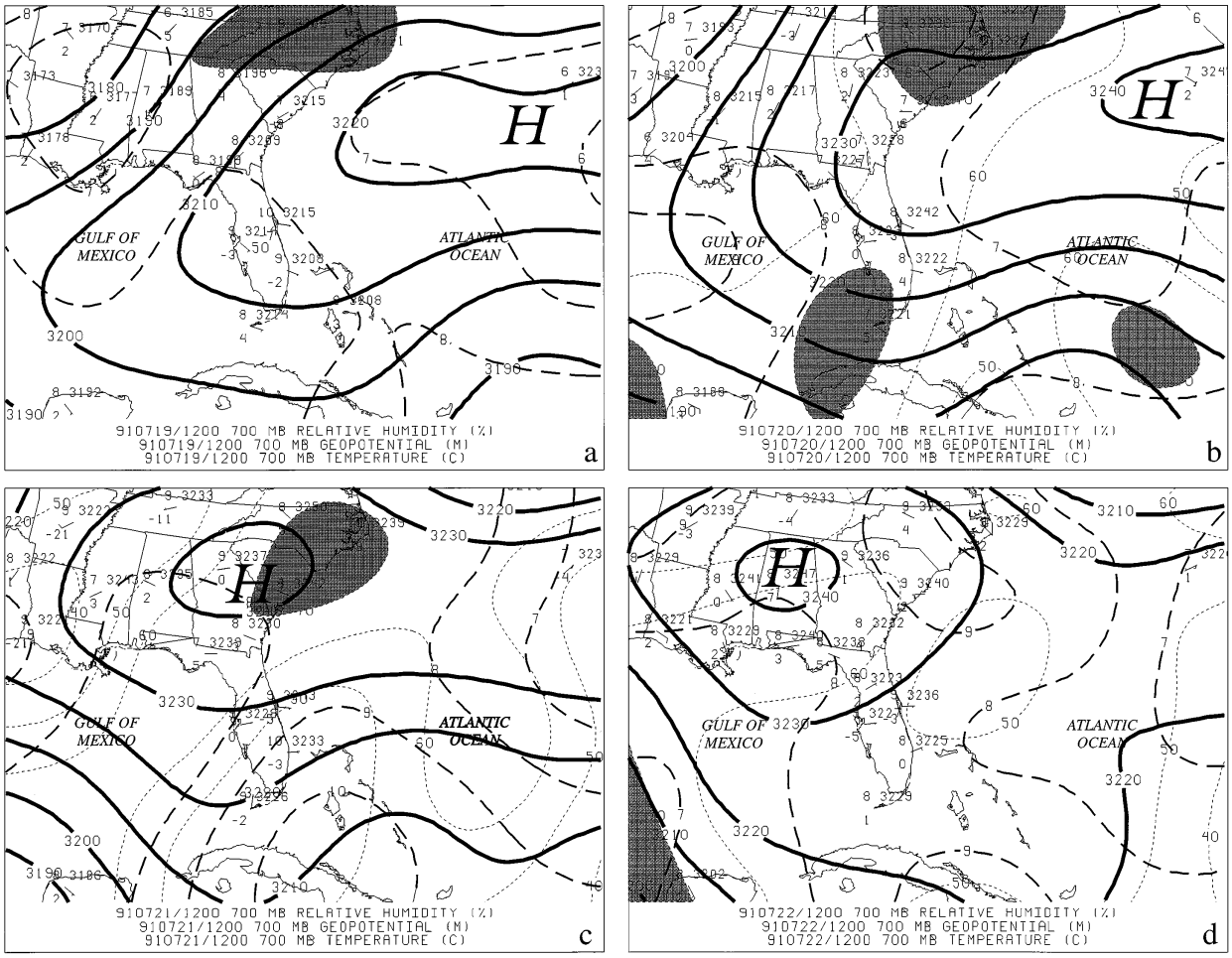

FIG. 4. Analyses of 700-mb geopotential heights (solid contours every 10 m), temperature (dashed contours every 1°C), and relative humidity ≥70% shaded for (a) 1200 UTC 19 July 1991, (b) 1200 UTC 20 July 1991, (c) 1200 UTC 21 July 1991, and (d) 1200 UTC 22 July 1991. The solid line from southeast Georgia to southeast Florida gives the location of the cross sections in Fig. 6. Station observations are plotted as temperature (°C) to the upper left of the station, dewpoint temperature (°C) to the lower left, geopotential height (m) to the upper right, and wind barbs where a half (full) barb equals 5 m s^{-1} (10 m s^{-1}).

days. Also, the 22 July sounding (Fig. 7b) shows a subsidence inversion near 760 mb, indicating greater stability on this day.

Of more significance is the moisture difference seen in the dewpoint profiles on the two days. The 20 July sounding (Fig. 7a) shows a deep moist layer from the surface to over 500 mb. The 22 July sounding (Fig. 7b) is decidedly drier, with a very shallow moist layer from the surface to about 900 mb and then dry above. The synoptic analysis for 1200 UTC on 22 July (Fig. 5d) shows the 150-mb jet streak over north Florida with convergence aloft producing the subsidence evidenced in this sounding. Model results presented in section 4 support this conclusion.

An analysis of CaPE and conventional soundings for convective available potential energy (CAPE), convective inhibition energy, and convective stability indices (Peppler 1988) found that only the K index, which references 700-mb moisture, was found to be of modest utility in discriminating convective activity in the vicinity of KSC on the 4 days investigated. However, it should be noted that the entire sounding should be examined closely by investigating multiple stability parameters in any convective situation.

To infer more information about the water vapor distribution and static stability, vertical cross sections of relative humidity and equivalent potential temperature were produced. The cross sections are based on the combined observational and numerical model analysis grids constructed for this research. Each cross section was drawn approximately perpendicular to the convective rainbands (refer to Fig. 1 for location). Relative humidity begins to increase between 1200 UTC 19 July and 1200 UTC 20 July (Figs. 8a and 8b). Deep moisture from KSC southeastward into the Bahamas is evident at 1200 UTC 20 July. The vertical extent of higher relative humidities (>70%) begins to decrease at 1200 UTC 21 July (Fig. 8c) and then remains rel-

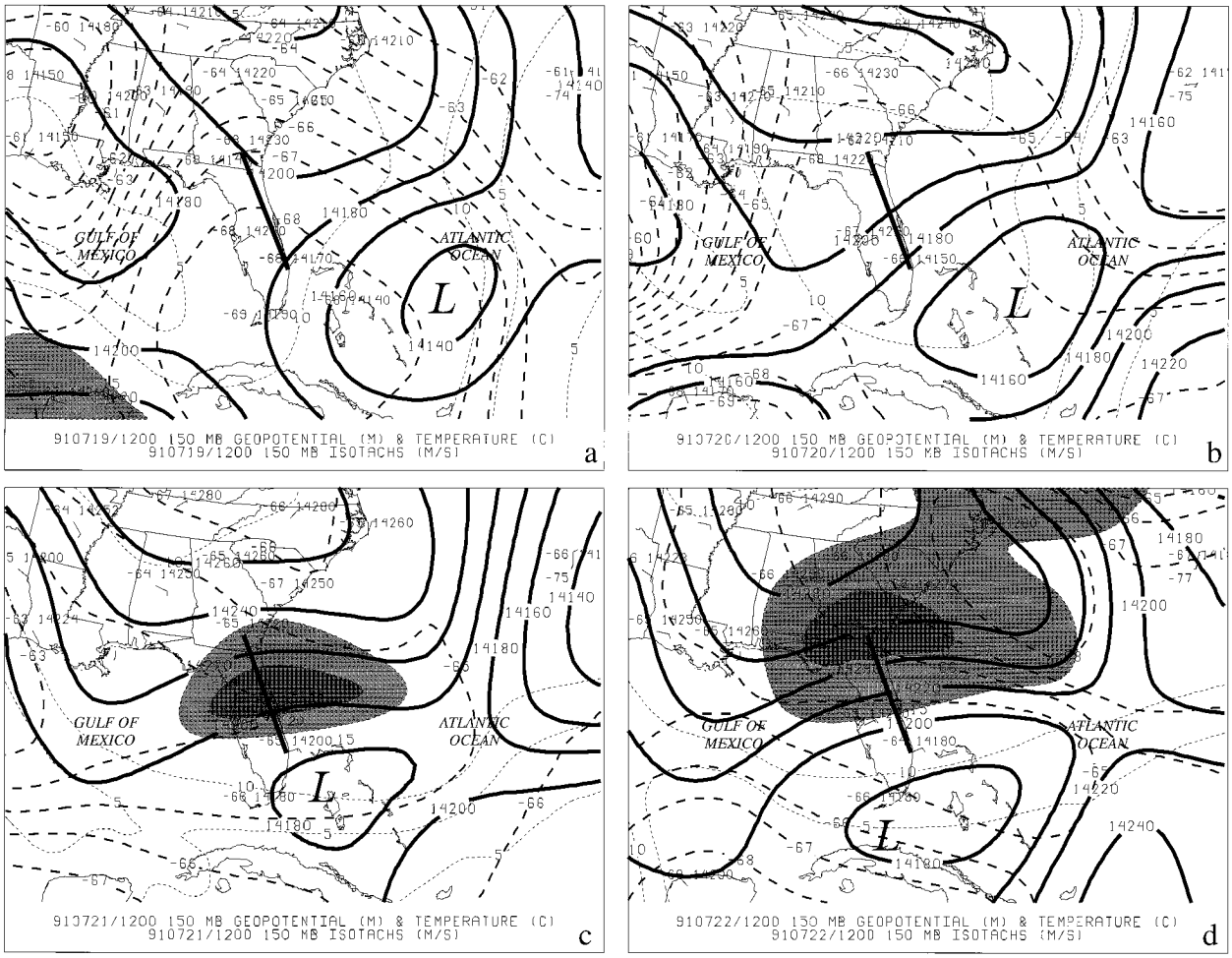

FIG. 5. As in Fig. 4 except for 150 mb depicting isotachs (every 5 m s^{-1}) shaded intervals beginning at 15 m s^{-1} and solid contours denoting geopotential heights (every 20 m).

atively shallow through 1200 UTC 22 July (Fig. 8d), providing qualitative agreement with observed convective activity.

Figure 9 shows *GOES-7* water vapor imagery in the 6.7-μm band. The 6.7-μm imagery is most sensitive to moisture and clouds in the middle and upper troposphere (Scofield and Purdom 1993) with a maximum sensitivity near 400 mb for a standard atmosphere, while for a dry upper atmosphere, the maximum sensitivity can be as low as 700 mb (Parke 1986). Thus, this wavelength is appropriate for helping define, qualitatively, the mid- and upper-level moisture patterns. The most prevalent feature in the water vapor images is the dark region extending across central Florida at 1200 UTC 21 and 22 July (Figs. 9c and 9d). The dark area extending parallel to the 150-mb wind maxima (see Fig. 5) strongly suggests drying of the upper-level air column associated with the downward vertical circulation induced by the jet streak (Anderson et al. 1982; Durran and Webber 1988). The drying associated with the wind maxima is consistent with subsidence and the suppression of convection on 21 and 22 July and provides evidence of the role of the upper-tropospheric dynamics.

In the absence of in situ data east of Florida, radar and satellite data provide the mesoscale data needed over the water to observe the initiation and structure of the convection. Visible satellite imagery reveals open cellular convection in the marine boundary layer on each of the 4 days (Fig. 2), indicating upward surface heat fluxes (Emanuel 1994). During active days, convection is observed to trigger at the apex of intersecting open cells, with new convection triggered by outflow boundaries.

Radar observations show that subsequently the convection becomes organized into rainbands. Radar observations were taken during CaPE, with single-Doppler scans from the National Center for Atmospheric Research (NCAR) CP-4 radar reaching up to 120 km offshore. The CaPE radars were turned on at ~1100 UTC each day, too late to see precipitation development for this case, but in time to observe rainband alignment and movement. The axes of the rainbands in the radar re-

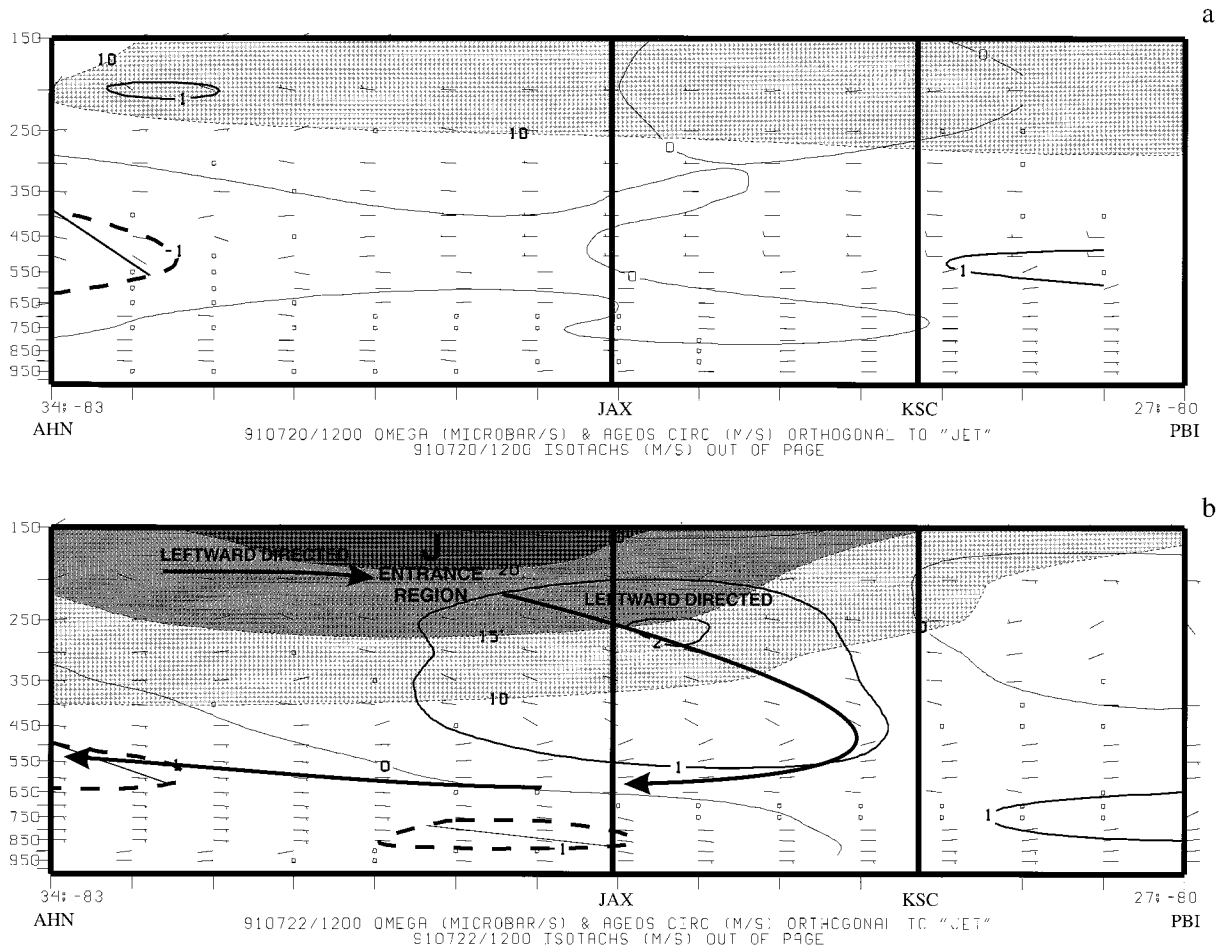

FIG. 6. Vertical cross sections for (a) 1200 UTC 20 July 1991 and (b) 1200 UTC 22 July 1991. The cross sections were taken orthogonal to the 150-mb jet streak (refer to heavy solid line in Fig. 1 for location). Areas of negative kinematic omega (upward motion) are cross hatched, and the heavy solid lines indicate areas of positive kinematic omega (downward motion). Isotachs are shaded in gray every 5 m s^{-1} beginning at 10 m s^{-1} and indicate flow out of the page. Wind barbs indicate the cross-stream ageostrophic circulation; half (full) barb equals 5 m s^{-1} (10 m s^{-1}). Solid black lines with arrows in (b) indicate transverse circulation pattern, and large ''J'' shows location of wind maximum.

flectivity scans all 4 days are parallel to the wind shear vector in the layer above the boundary layer (see Fig. 10). On 20 July, the bases of the convective rainbands were about 925 mb and the tops were about 535 mb. The inset in Fig. 10 shows one of the rainbands from the radar reflectivity plot. The rainband is oriented with its length parallel to the wind shear over the depth of the rainband (longitudinal mode). Also, the rainbands moved perpendicular to the wind shear over the depth of the rainband and were stationary relative to the mean flow.

e. Instability parameters

Four convection initiation processes were considered to explain the organization of the convective rainbands. These include conditional symmetric instability (CSI), inflection point instability (IPI), wave-CISK (conditional instability of the second kind), conventional static stability, and the effects of moisture distribution on suppressing convection initiation (Emanuel 1994).

Following Bennetts and Hoskins (1979), analyses of available data indicate that CSI was not a mechanism responsible for the organization of the rainbands. Given the lack of baroclinicity in the larger-scale environment, this result was expected. CCAS soundings were used to produce profiles of the mean winds parallel (along roll) and perpendicular (cross roll) to the orientation of the rainband. An inflection point is observed at about 1300–2000 m each day in the rotated *u*-component profile [along roll; Lemone (1973)]. Since the inflection point is in the along-roll direction, it is unlikely that IPI is responsible for rainband development or alignment, but IPI could be responsible for the observed spacing of the convective cells along the rainbands (e.g., Businger and Hobbs 1987). Modeling results agree with these observations and show IPI in the along-roll direction in the nested grid simulations (not shown).

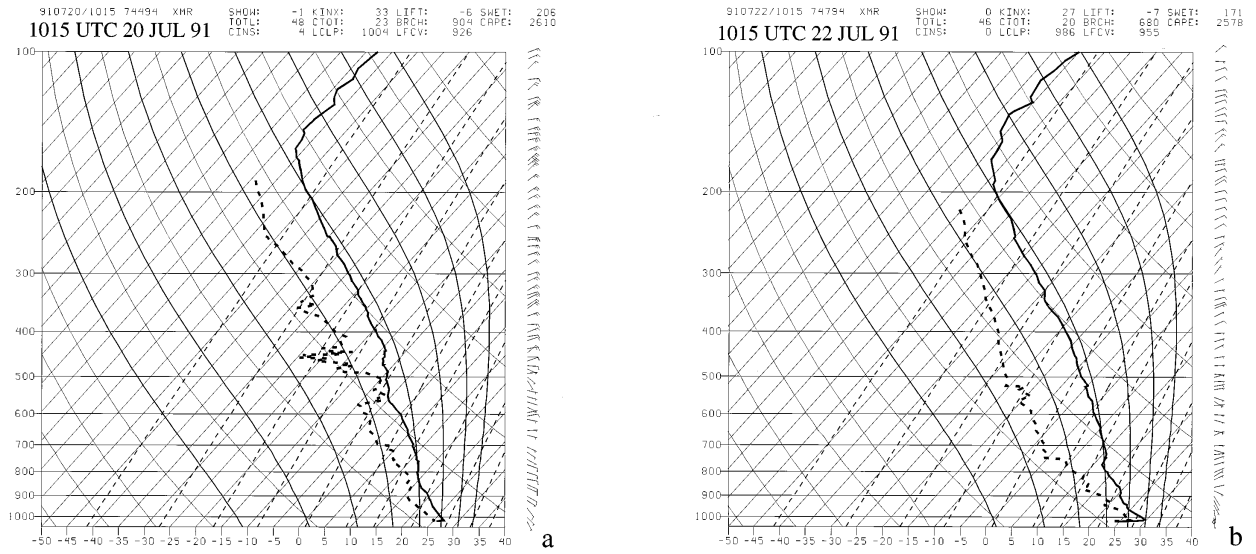

FIG. 7. Standard skew *T*–log *p* diagrams of soundings for Cape Canaveral Air Station at (a) 1015 UTC 20 July 1991 and (b) 1015 UTC 22 July 1991. Temperature curve is heavy solid line; dewpoint curve is heavy dashed line. Dry adiabats are the slightly thin curved lines that run diagonally upward from right to left, saturated adiabats are the thin curved lines diverging upward and tending to become parallel to the dry adiabats, isotherms are the thin straight lines running diagonally upward from left to right and are labeled every 5°C along the bottom of the skew *T*, the saturation mixing ratio is represented by the thin dashed lines running diagonally upward from left to right, and the isobars are straight thin horizontal lines labeled every 100 mb on the left of the skew *T*. Wind barbs show where a half (full) barb equals 5 m s^{-1} (10 m s^{-1}).

Lindzen (1974) defines wave-CISK as motions that do not require Ekman pumping in order to produce CISK. This class of motions includes those associated with internal waves such as gravity, Kelvin, mixed gravity–Rossby, and Rossby. Sun (1978) included latent heat effects in linear models following the wave-CISK hypothesis proposed by Lindzen. Sun determined that the orientation and speed of the rainbands varied based on the dominance of buoyancy-generated heat release or the conversion of kinetic energy from the mean flow. If buoyancy dominates, then the rainbands are oriented parallel to the wind shear in the layer and remain stationary relative to the mean flow in the rainband layer (e.g., Businger and Walter 1988). This minimizes the tendency of the shear to suppress convection. As previously discussed, the rainbands were oriented parallel to the wind shear in the layer and were stationary relative to the mean flow as the buoyancy mode of wave-CISK would suggest. Therefore, it is likely that wave-CISK played a role in development, maintenance, and propagation of the convective rainbands observed in this case.

4. Description of the Mesoscale Atmospheric Simulation System

Numerical simulations were produced by MASS, a hydrostatic atmospheric model based on a set of equations consisting of seven prognostic variables: temperature, water vapor mixing ratio, *x*—space, *u*—wind component, *y*—space, *v*—wind component, surface pressure, cloud water/ice mixing ratio, and rainwater/snow mixing ratio (MESO, Inc. 1995). The original version of MASS used in this research was developed by Kaplan et al. (1982) and later modified to the Goddard Mesoscale Atmospheric Simulation System (Manobianco et al. 1996). The version of MASS used in this research was developed by MESO, Inc., and includes a prognostic grid-scale moisture scheme, an enhanced surface energy budget, a modified Kuo cumulus parameterization scheme that includes convective scale downdrafts, and a more comprehensive long- and shortwave radiation scheme (Zack et al. 1991; MESO, Inc. 1995; Manobianco et al. 1996). Additional improvements to the MASS convective parameterization and surface physics were made during 1992 and the early portion of 1993, followed by replacement of the objective analysis scheme (Barnes 1964) with a three-dimensional multivariate optimal interpolation (3D OI) scheme in 1995 (MESO, Inc. 1995). MASS was run on a workstation at North Carolina State University (NCSU) under similar computational conditions as those at CCAS with the intent of showing a capability for operational forecasting for easterly flow situations.

Zack et al. (1988 and 1991) showed the effectiveness of MASS in simulating convective cloud systems over Florida and in forecasting thunderstorms at KSC. The Applied Meteorology Unit (AMU), which is collocated with Range Weather Operations at (CCAS), has been evaluating MASS since it was delivered by MESO, Inc., in March 1993 for application as a real-time forecasting tool for use by Range Weather Operations in support of

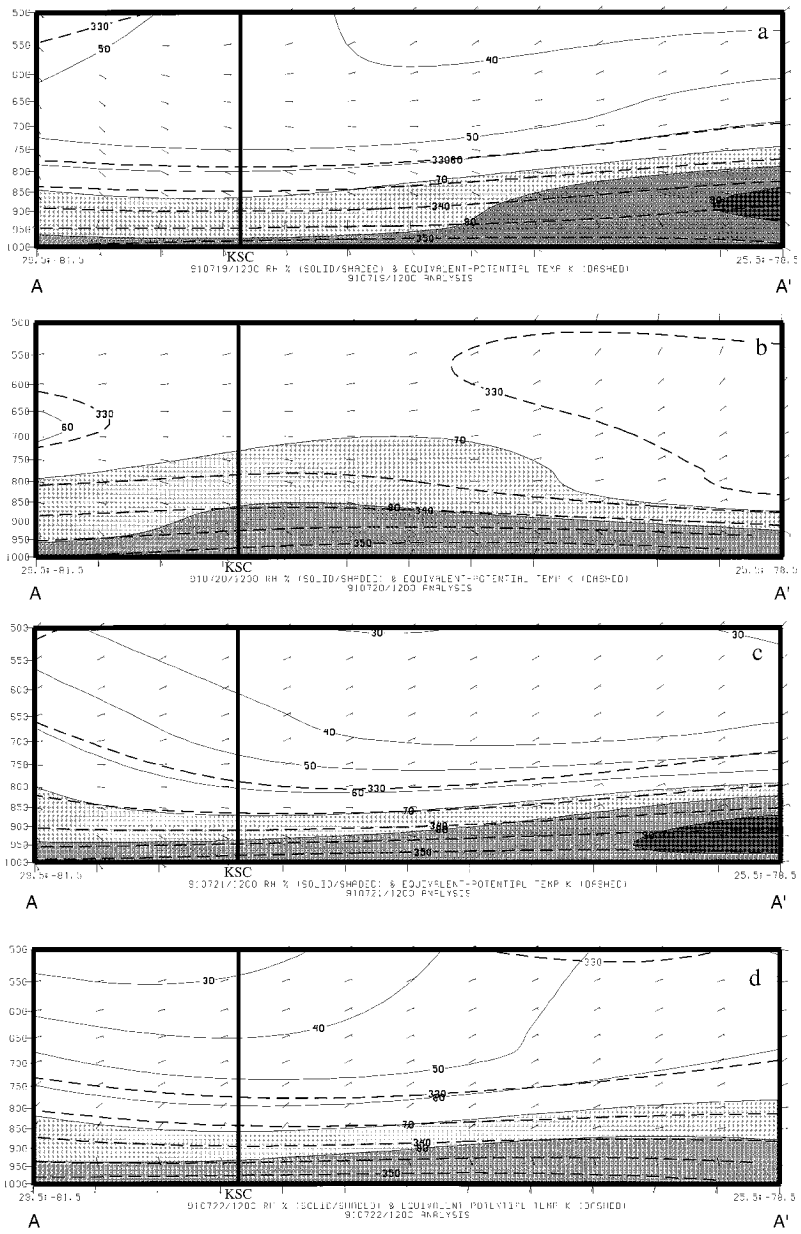

FIG. 8. Cross section of relative humidity (progressive shading every 10% for RH > 70%) and equivalent potential temperature (dashed lines every 5 K): (a) 1200 UTC 19 July 1991, (b) 1200 UTC 20 July 1991, (c) 1200 UTC 21 July 1991, and (d) 1200 UTC 22 July 1991. Refer to heavy dashed line A–A′ in Fig. 1 for location.

all space launch activity from KSC and CCAS. Since April 1995, MASS has been used on a limited operational basis by Range Weather Operations forecasters. Due to extensive AMU experience using MASS for Florida space shuttle support, their coarse mesh was matched. Then, sensitivity tests were conducted using a fine mesh (nest) designed specifically for the onshore flow regime (Fig. 11). The nested MASS model grids used in this research are similar to the AMU's, but the areal coverage is larger, especially to the east of Florida (Fig. 11).

a. Coarse grid simulation

The coarse simulations were run once for each of the 4 days (19–22 July) for comparison with objective analyses and for use as the first-guess field in the nested simulations. The coarse MASS grid is identical to the AMU coarse setup with 45 km horizontal grid spacing and 22 vertical sigma levels. Operationally, the AMU uses the NGM, with 80-km horizontal grid spacing, as the first-guess data source and forecast lateral boundary condition source. For this research, archived GOI, with

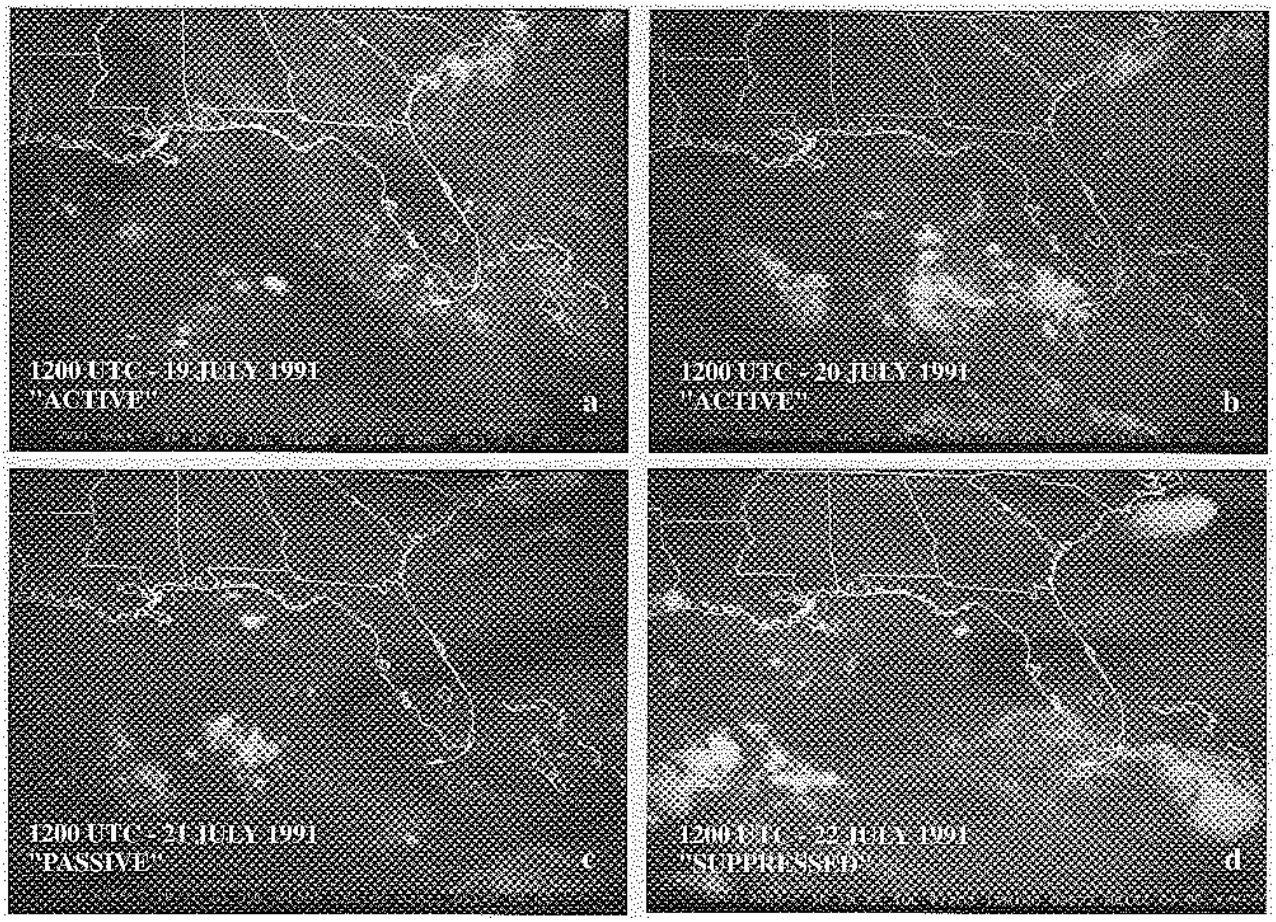

FIG. 9. Water vapor (6.7-μm band) satellite imagery (8-km horizontal resolution) from *GOES-7* for (a) 1200 UTC 19 July 1991, (b) 1200 UTC 20 July 1991, (c) 1200 UTC 21 July 1991, and (d) 1200 UTC 22 July 1991.

2.5° × 2.5° latitude–longitude resolution, was used as the first-guess data source and forecast lateral boundary condition source. Archived NGM data were not used in this study because the data are only available up to 300 mb. Other data sources used in this study are the same as used at the AMU and include rawinsondes and surface observations [consisting of Meteorological Interactive Data Display System land report format conventional hourly surface observations, KSC tower mesonet, and KSC buoy and ship report format].

Two changes to the model parameters that differ from the AMU setup were the inclusion of high-resolution (9-km grid spacing) weekly averaged sea surface temperatures (SST) from polar orbiter satellites and the use of prognostic moisture physics in the microphysics scheme (the AMU uses diagnostic moisture physics due to computational restrictions). If any of the high-resolution SST data were missing, it was replaced by the climatological SST. In the diagnostic moisture scheme, no liquid or frozen water is retained in the atmosphere, while the prognostic moisture scheme incorporates prediction equations for cloud water and cloud ice and rain-snow water. The prognostic moisture scheme models the atmospheric water cycle in greater detail than the diagnostic moisture scheme but is much more computationally intensive. The initialization time for the coarse grid simulations was 0000 UTC for each of the 4 days, and the model ran for 24 h with output at 1-h intervals.

In comparing model output with the observational analyses, 12-h MASS predictions correctly build the surface ridge westward and develop a closed high by 1200 UTC 22 July (Fig. 12). At 700 mb (Fig. 13), anticyclonic curvature prevails over Florida with the ridge slowly migrating northward until a closed high develops at 1200 UTC 21 July (Fig. 13c). Similar to the observational analyses (Fig. 4), simulated heights rise an average of 40 m over the southeast United States through the period, consistent with the development of low-level divergence over the region that helps to suppress convection later in the period. Areas of high relative humidity (>70%) are more prevalent in the MASS output, but the basic patterns of relative humidity match well on all four days.

At 150 mb, the general position of the TUTT is well simulated by MASS (Fig. 14). Moreover, the evolution of the geopotential height gradient and a 20 m s^{-1} jet

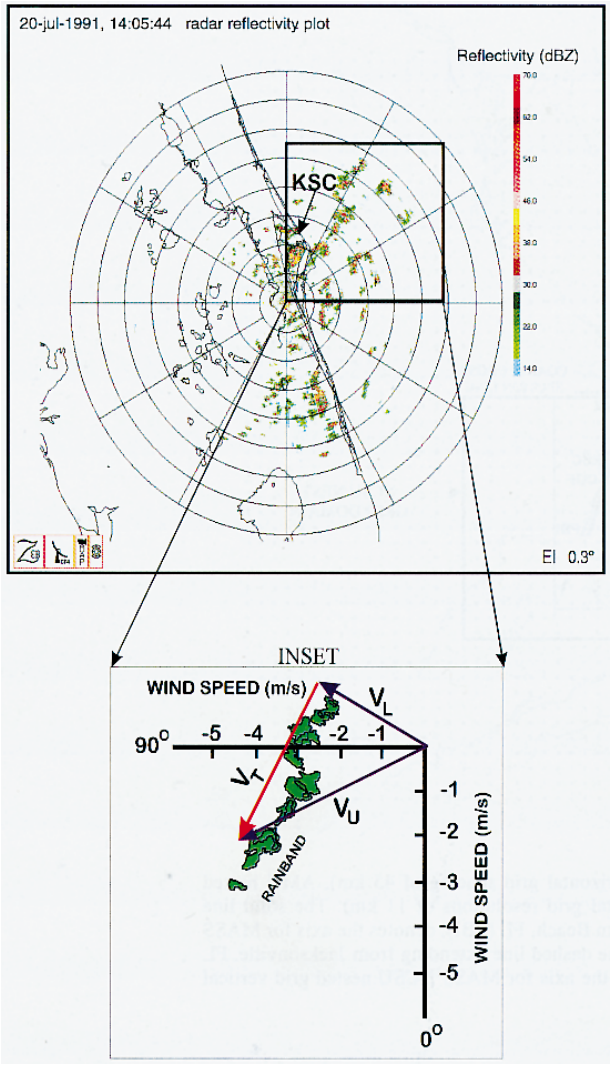

FIG. 10. Plan Position Indicator view of reflectivity from the CP-4 Doppler radar for 1405 UTC 20 July 1991. The inset shows the rainband alignment parallel to the wind shear vector ($V_T - V_B$) in the rainband layer where V_T is the wind vector at the top of the rainband layer (535 mb) and V_B is the wind vector at the bottom of the rainband layer (925 mb).

streak that forms over northern Florida on 21 and 22 July are captured well by MASS. Consistent with jet streak dynamics, the MASS simulation produces upper-level divergence over Florida on 19 and 20 July, when the convection was active, and upper-level convergence over central Florida on the suppressed days, 21 and 22 July.

The jet streak dynamics can be investigated by looking at vertical cross sections orthogonal to the jet as it develops and moves westward across Florida. The cross section for 19 July (Fig. 15a) shows little organization to the circulation, and no jet streak is evident. On 20 July (Fig. 15b), the cross section shows the jet exit region centered at 200 mb over JAX. The ageostrophic motion is rightward (northward) directed in the upper troposphere as expected in this region of the jet streak. The transverse circulation throughout the troposphere shows downward vertical motion near AHN (Fig. 1) associated with the right exit region of the jet and upward vertical motion from KSC south to PBI (Fig. 1) in the left exit region of the jet. The position of the jet streak and transverse circulation implicitly support the convection observed on 20 July.

On 21 July, the center of the jet streak is located between KSC and JAX (Fig. 15c). The jet exit region is now west of KSC and the entrance region is east of KSC. The KSC weather was defined as passive since weak convection was observed early in the morning giving way to more suppressed conditions later in the morning. The transition of the weather from active to suppressed closely parallels the movement of the jet streak across the KSC area. By late morning, KSC weather was beginning to be influenced by the left entrance region of the jet streak (cyclonic side) resulting in upper-level convergence and downward motion south of the jet streak. By 22 July, the KSC area weather is influenced by the left entrance region of the jet streak as it has moved north of JAX (Fig. 15d) and into northern Florida and Georgia (Fig. 14). The transverse circulation shows leftward- (southward-) directed motion in the upper troposphere and a return flow northward at lower levels.

The MASS coarse grid simulations are consistent with the observational analysis and jet streak model presented in section 3. A higher-resolution nest was run to evaluate the ability of MASS to simulate mesoscale precipitation structures.

b. Nested grid simulations

The nested MASS grid was run with 11-km horizontal grid spacing with 22 vertical sigma levels (identical to the AMU nest setup) to evaluate the impact of the higher-resolution grid in simulating the observed mesoscale structure. The cumulus scheme used was Kuo–Meso, which has been shown to work well at these nested resolutions (Zack et al. 1988, 1991). The nested simulations were run six times for each of the 4 days to determine if it could duplicate the water vapor distribution observed in the analyses. The MASS coarse grids were used as the first-guess fields for the 24 nested simulations. The main differences between setup of the AMU nest and the NCSU nest were the grid domain size (Fig. 11) and the use of high-resolution (9-km grid spacing) SST in this research. Because easterly flow is the focus of this work, the nested grid was expanded eastward by 297 km and southward by 77 km and reduced on the west side by 66 km and the north side by 22 km. The initialization time was 0600 UTC, and the model ran for 12 h with output at 1-h intervals. Analysis

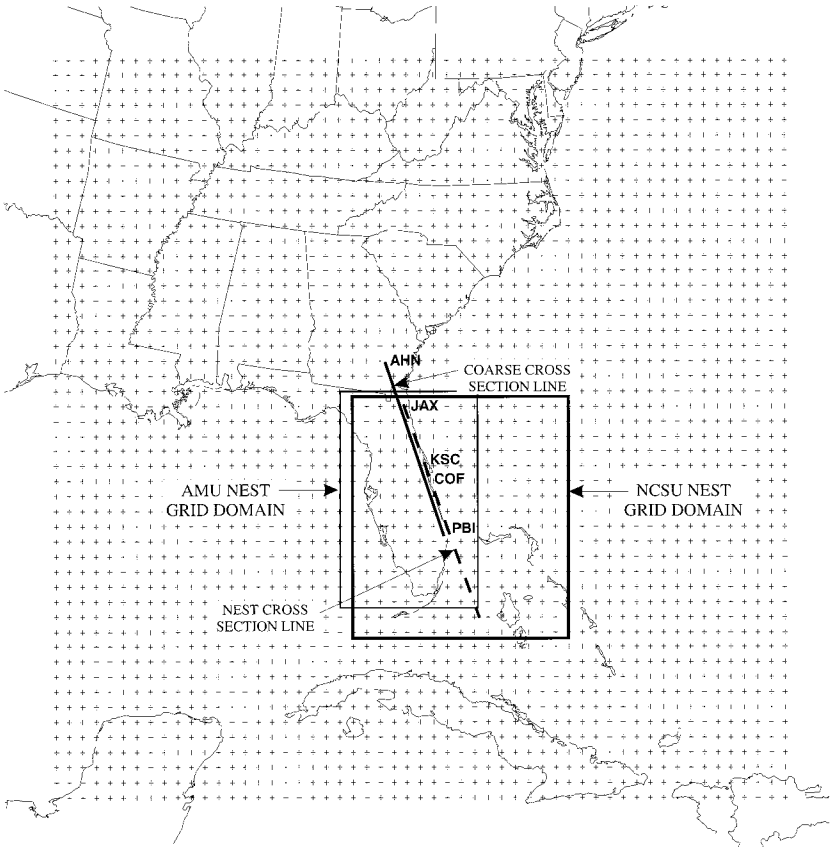

FIG. 11. The MASS coarse grid domain (horizontal grid spacing of 45 km), AMU nested grid domain, and NCSU grid domain (horizontal grid resolutions of 11 km). The solid line extending from Athens, GA (AHN), to West Palm Beach, FL (PBI), denotes the axis for MASS coarse grid vertical cross sections in Fig. 15. The dashed line extending from Jacksonville, FL (JAX), to west of the Bahamas Islands denotes the axis for MASS NCSU nested grid vertical cross sections in Figs. 16, 21, and 22.

of model output concentrated on the 6-h forecast valid at 1200 UTC each day to match the times of observational and coarse grid analyses. The initialization data sources were the same as the coarse grid except for rawinsonde data, which are unavailable at 0600 UTC. Vertical cross sections were constructed approximately orthogonal to the rainbands from near JAX through KSC and Patrick Air Force Base (COF) to just west of the Bahamas (see Fig. 11).

The two most contrasting weather days, 20 and 22 July, are shown for comparison. At 1200 UTC 20 July the MASS nested grid forecast (Fig. 16a) shows the strongest upward vertical motion located under the left exit region of a well-developed jet streak consistent with the observational analyses and coarse grid simulation. Upward vertical motion is greatest and deepest at this time and is organized in a banded structure. The satellite imagery at this time shows four developing convective rainbands (Fig. 2b). One is just northeast of KSC, one offshore and adjacent to COF, and two others southeast of COF. The cross section shows the jet streak in about the same position as the coarse grid simulation (near JAX and at about 200 mb).

At 1200 UTC 22 July, the MASS forecast shows the jet streak entrance region, with upper-level convergence and subsidence, over KSC (Fig. 16b). Although little downward vertical motion is seen in the cross section, the upward vertical motion is considerably weaker than on previous days and covers a much smaller area. The strongest upward motion is at the southernmost part of the cross section where strong thunderstorms associated with an upper-level cold-core low were occurring at this time. The satellite image for this time shows only the open-cell boundary layer convection present with the suppressed conditions (Fig. 2d).

c. Nested grid moisture enhancement sensitivity studies

The representation of relative humidity in MASS is critical for determining how well the model can forecast water vapor distribution during onshore flow. Since ra-

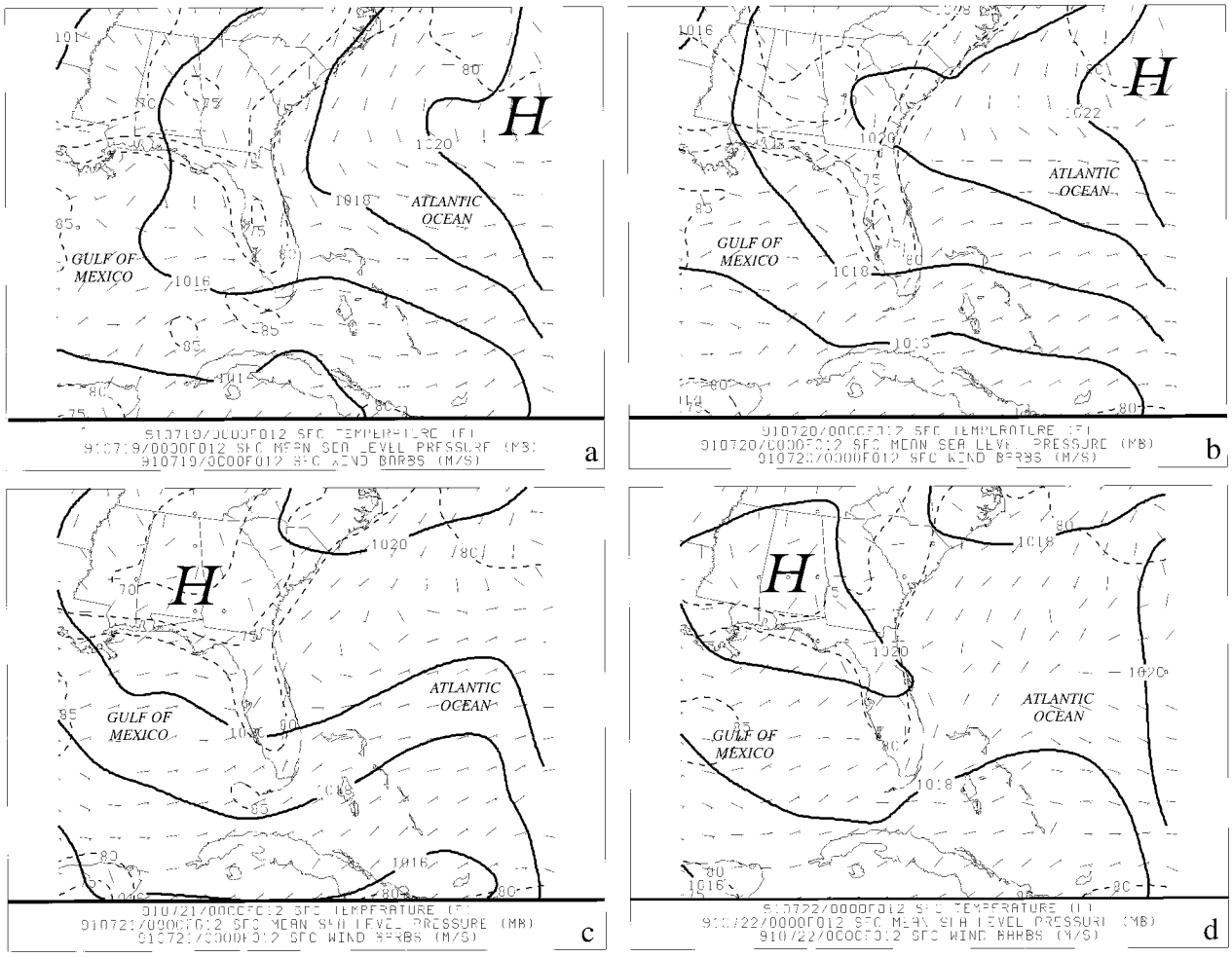

FIG. 12. MASS 12-h coarse grid forecasts of mean sea level pressure (solid contours every 2 mb), temperature (dashed contours every 5°F), and wind barbs (half) equal 10 m s^{-1} (5 m s^{-1}) for (a) 1200 UTC 19 July 1991, (b) 1200 UTC 20 July 1991, (c) 1200 UTC 21 July 1991, and (d) 1200 UTC 22 July 1991.

winsonde data are not a sufficient source of moisture data for MASS, the model allows for inclusion of derived moisture in the initialization. The MASS synthetic relative humidity scheme (MESO, Inc. 1995) allows for enhancement of the relative humidity analysis from manually digitized radar (MDR) data, satellite imagery, and visual observations of clouds (surface observations). Since these derived sources of data do not measure or report relative humidity values, the vertical profile of relative humidity must be inferred at a given location. This information is then used to enhance the rawinsonde data for use in the model.

To insert these moisture sources into MASS, one of the MASS modules ingests a model-ready initialization file and changes the relative humidity field based on the information inferred from the three sources of moisture data. The module then outputs a new initialization file containing the updated relative humidity fields but leaves all other variables unchanged.

d. Enhancement with MDR

Gridded analyses of areal coverage of precipitation and radar video integrator processor (VIP) levels (National Oceanic and Atmospheric Administration 1982) provide estimates of rainfall rates for MASS. The VIP levels are assigned a value at the nearest MDR grid point, having a 40-km horizontal grid spacing. To help reduce the spreading of isolated convection on the grid and before the values are assigned to the MASS grid, the data are processed to set grid points with VIP levels ≤ 2 equal to zero, if they are located between a convective core (VIP ≥ 4) on one side and to an echo-free grid point (VIP $= 0$) on the other. To estimate cloud tops when infrared satellite imagery data are unavailable, MASS will use the MDR data and the relationship where

$$\sigma_{\text{top}} = 0.7 - 0.11(\text{VIP})^{0.91} \quad (1)$$

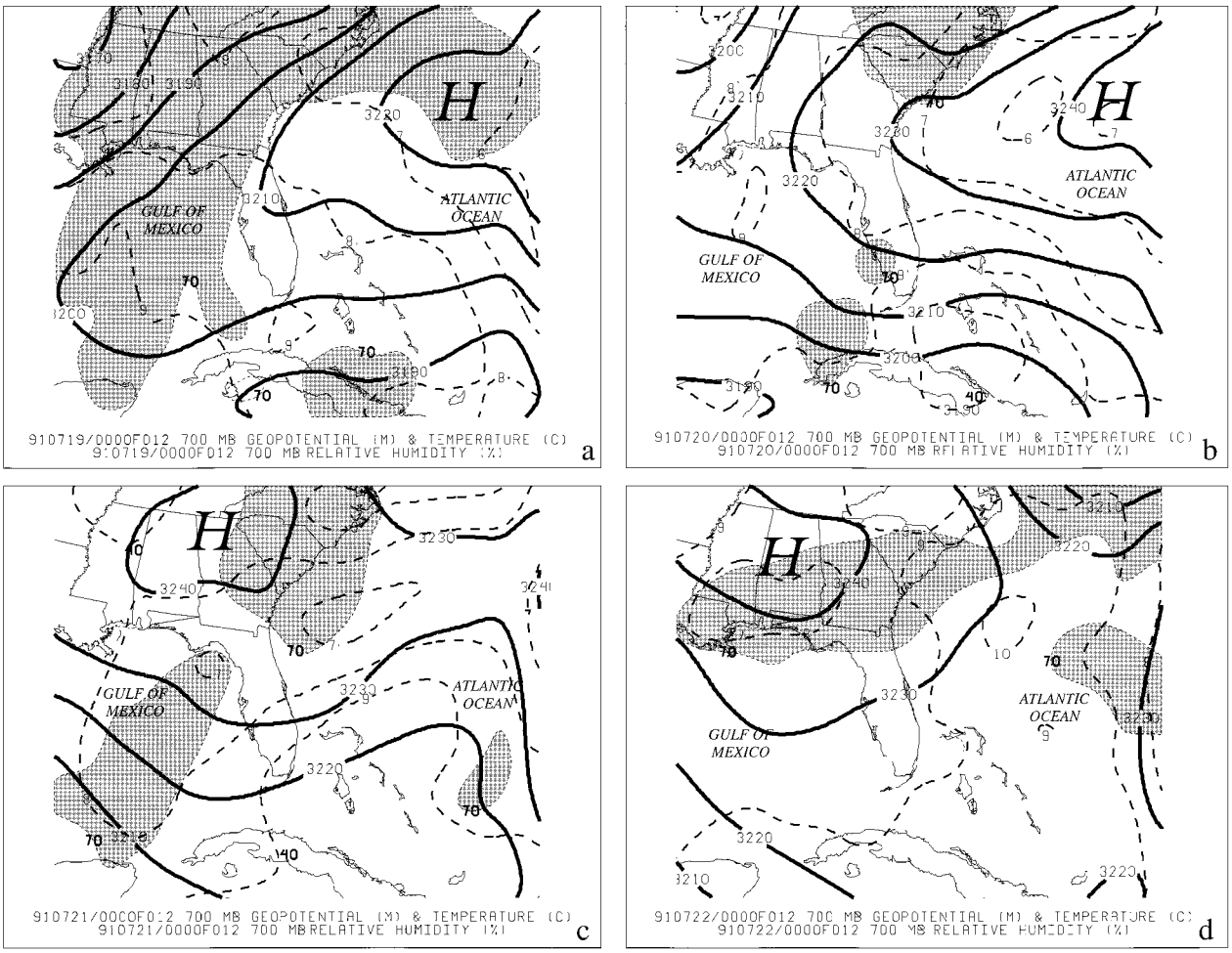

FIG. 13. MASS 12-h coarse grid forecasts of 700-mb geopotential heights (solid contours every 10 m), temperature (dashed lines every 1°C), relative humidity ≥70% shaded, and wind barbs (half) equal 10 m s^{-1} (5 m s^{-1}) for (a) 1200 UTC 19 July 1991, (b) 1200 UTC 20 July 1991, (c) 1200 UTC 21 July 1991, and (d) 1200 UTC 22 July 1991.

and σ_{top} is the top of the model domain or 100 mb (MESO, Inc. 1995).

e. Enhancement with infrared satellite imagery

The infrared (IR) satellite imagery is used to determine the amount of cloud cover in each grid box. The scheme incorporated in MASS is a simplified version of the one used by Hamill et al. (1992). A cloud is detected if $\Delta T_{\text{obs}} = T_{\text{cir}} - T_{\text{obs}} \geq T_{\text{thresh}}$, where T_{cir} estimates the brightness temperature that the satellite would measure under clear skies, T_{obs} is the IR brightness temperature the satellite observes, and T_{thresh} is an uncertainty in the estimate of T_{cir} and because T_{obs} is likely to be large when clouds are present in a relatively dry, unstable atmosphere (MESO, Inc. 1995). With use of the IR data, the height of the topmost cloud layer is calculated by matching cloud-top brightness temperatures with atmospheric temperatures from the rawinsonde analysis. The cloud base is estimated in one of two ways. If surface data are available and the cloud coverage is ≥80%, MASS assumes the cloud base coincides with the highest broken or overcast cloud base at the nearest surface station. If surface data are unavailable or cloud coverage is <80%, MASS assumes the cloud base to be 500 m below cloud top (MESO, Inc. 1995).[1] The satellite imagery also dries cloud-free

[1] If radar data and surface observations are unavailable, essentially nothing is known about the cloud base. Some sort of assumption about the thickness of the clouds needs to be made. The clouds could be considerably thinner than 500 m and still appear opaque in the IR satellite image. However, the model layers are typically 1 km thick or even thicker at mid- to upper levels. The problem is trying to simulate the radiative and other important properties of thin clouds that cannot be resolved. At the other end of the spectrum, the clouds could be several kilometers thick. At some point they would be likely to be precipitating and a radar echo would be present to help in the decision making process. Lacking that information, 500 m seemed to be a good compromise. With the coarse vertical resolution we

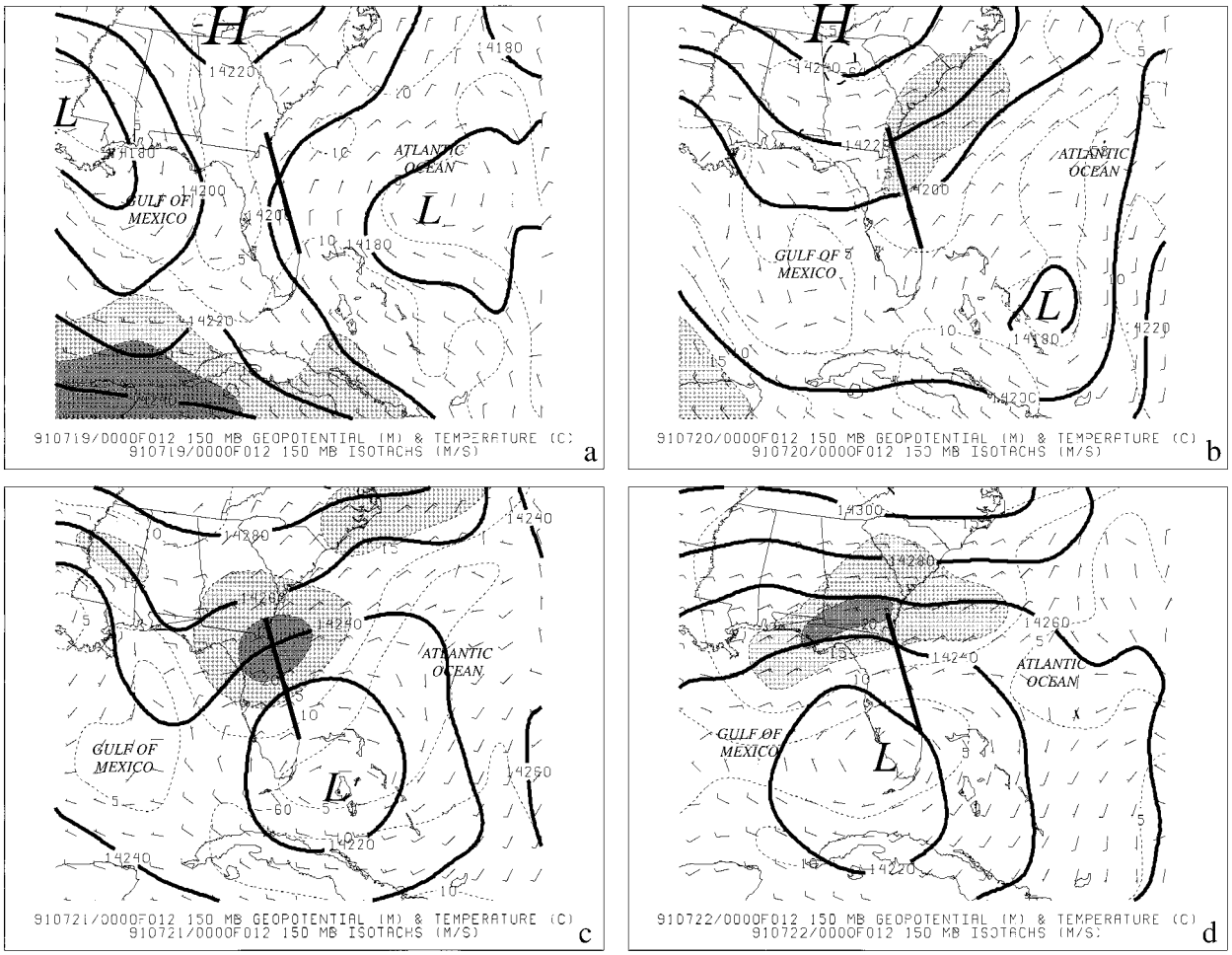

FIG. 14. MASS 12-h coarse grid forecasts of 150-mb geopotential heights (solid contours every 20 m) and isotachs (thin dashed lines every 5 m s^{-1}, with areas >15 m s^{-1} progressively shaded) for (a) 1200 UTC 19 July 1991, (b) 1200 UTC 20 July 1991, (c) 1200 UTC 21 July 1991, and (d) 1200 UTC 22 July 1991. Wind barbs (half) equal 10 m s^{-1} (5 m s^{-1}). Heavy straight line indicates location of cross sections in Fig. 15.

areas. This is a critical procedure that significantly affected the results of moisture enhancement in this work and will be discussed later. The maximum relative humidity is set to 75% above cloud tops. At any point where the satellite-determined cloud fraction is $<100\%$ but $>5\%$, the relative humidity at any given level cannot exceed the value calculated from

$$\mathrm{RH} = \frac{(3.0 + C^{0.33})}{4.0}, \qquad (2)$$

where C is the areal coverage and relative humidity (RH) = 1 at saturation (MESO, Inc. 1995). At any point having a satellite-determined cloud fraction of $<5\%$, the relative humidity at any given level cannot exceed the mean plus one standard deviation of the relative humidity from the clear skies category in the statistical database (MESO, Inc. 1995). The final part of the satellite data enhancement is a scheme after Adler and Negri (1988) to locate convective towers. This scheme in MASS finds all of the IR temperature minima and then calculates a slope parameter for each temperature minima. Each convective tower is assumed to represent a 64 km^2 saturated region.

f. Enhancement with surface-based observations

Surface observations are placed into cloud/weather categories based on the height of each cloud layer, the cloud coverage, and the preceding hour's weather. Cloud

would only be moistening one layer even with a 1000-m thickness. So the minimum cloud thickness assumption will only result in the moistening of one model level. This was a far better compromise than the possibility of introducing a spurious thick cloud, or not moistening at all when clearly there is a cloud. Finally, the algorithm that detects convective towers should detect MCSs or tropical cyclones, so the 500-m thickness assumption would not be applied in this case (S. Young 1996, personal communication).

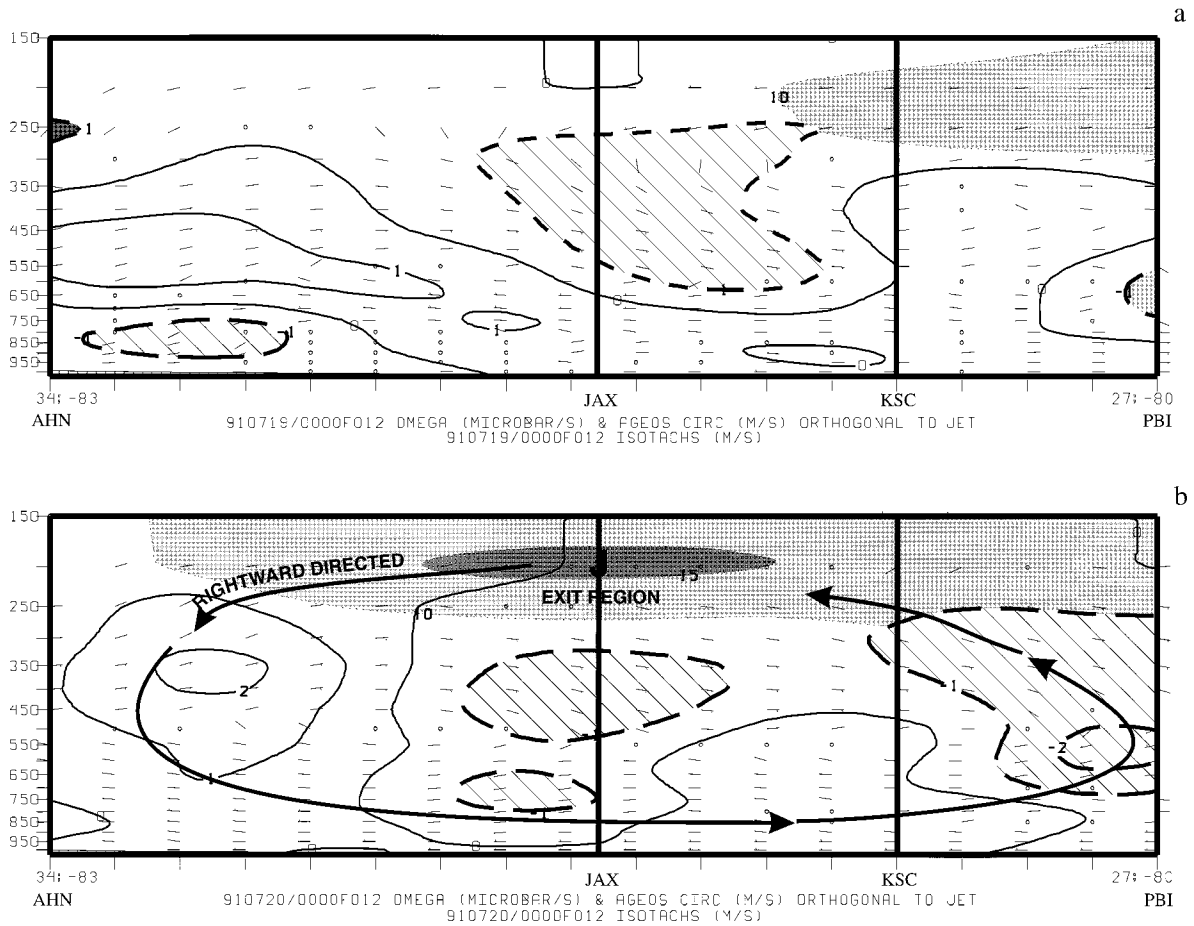

FIG. 15. Vertical cross sections of MASS 12-h coarse grid forecasts for (a) 1200 UTC 19 July 1991, (b) 1200 UTC 20 July 1991, (c) 1200 UTC 21 July 1991, and (d) 1200 UTC 22 July 1991. Cross sections were taken orthogonal to the 150-mb jet streak (see Fig. 14 for location). Areas of negative kinematic omega (upward motion) are cross hatched, and heavy solid lines indicate areas of positive kinematic omega (downward motion). Isotachs are progressively shaded in gray every 5 m s^{-1} beginning at 10 m s^{-1} and indicate flow out of the page. Wind barbs indicate the cross-stream ageostrophic circulation; a half (full) barb equals 5 m s^{-1} (10 m s^{-1}). Solid black lines with arrows indicate transverse circulation pattern. Large ''J'' shows location of wind maximum.

bases $<$1250 m above ground level are classified as low cloud, cloud bases $\geq$1250 m and $\leq$4700 m above ground level are classified as middle cloud, and cloud bases $>$4700 m above ground level are classified as high cloud. The cloud coverage is classified as scattered, broken, or overcast. The weather is also classified into three categories: precipitation, no precipitation, or fog. After the surface observation is classified, the relative humidity in a collocated sounding is interpolated to 32 levels starting at the surface and incremented every 25 mb. Datasets were created and used to derive the statistical prediction equations of relative humidity values for each level in each cloud/weather category. A root-mean-square error is used to identify levels that have a satisfactory correlation, and when the error is $<$15%, the levels meeting the criteria are blended into a rawinsonde analysis using the Barnes (1964) analysis scheme. The rawinsonde analysis is a statistical analysis based on a dataset of 5876 rawinsondes used by the MASS synthetic relative humidity scheme for surface-based observations (MESO, Inc. 1995).

g. Moisture enhancement of the NCSU nested grid

Sensitivity studies were conducted using the nested grid with moisture enhancement from three different sources using five different schemes. First, a baseline nest was run using the AMU grid and parameters with no moisture enhancement. The baseline run was compared to a basic (no moisture enhancement) run using the NCSU nested grid, which included high-resolution (9-km grid spacing) SST data. The AMU baseline run and the NCSU basic run water vapor distribution agreed quite well when comparing relative humidity and average convective precipitation output. Relative humidity at 700 mb was nearly identical over Florida, but the AMU baseline missed some higher values just east of Florida, probably due to the smaller grid domain used

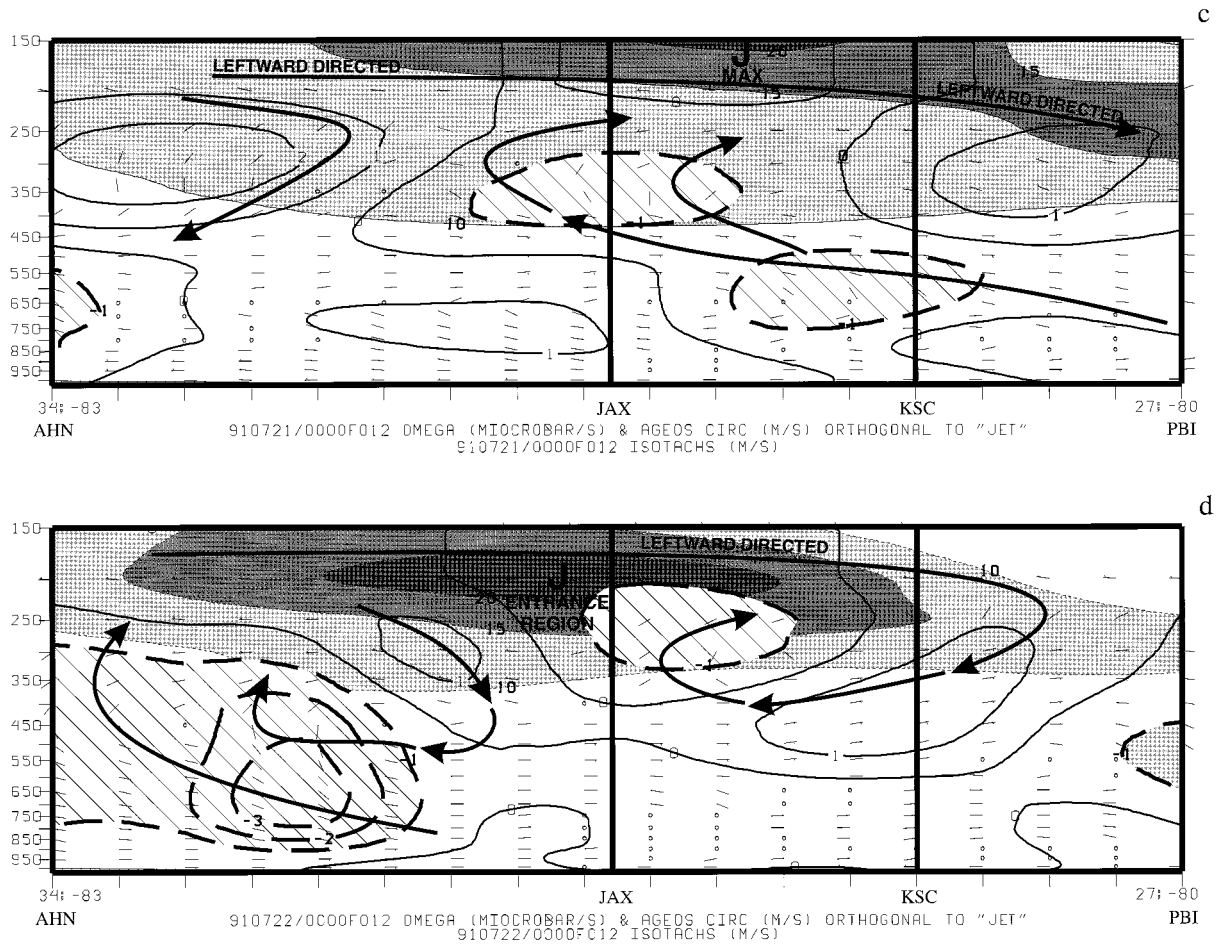

FIG. 15. (*Continued*)

in the AMU baseline. The AMU baseline run produced less precipitation, averaged over 6 h, than the NCSU basic run, but generally placed it in the same region.

The rest of the NCSU nested runs consisted of including the derived moisture from one source and running a simulation with only that source. Then the derived moisture from the next source would be used and a simulation run with only that source. Once runs were completed with each individual source, all the derived moisture sources were included in the last simulation. The moisture sources that were introduced include MDR data with 40-km grid spacing (Fig. 17), *GOES-7* infrared satellite imagery with 4-km resolution (Fig 18), and cloud observations from conventional surface observations (Fig 19). Since the 700-mb RH analyses are too coarse to show the small-scale water vapor distribution from the MASS nested grid, the model-generated 700-mb relative humidity forecast was compared to the 4-km IR satellite images valid at the same time (not shown, see Fig. 2 for corresponding visible imagery) to gauge the effects of moisture enhancement into MASS.

The MDR significantly increased the relative humidity and precipitation on all days in areas where radar echoes were detected at initialization time. Unrealistic widespread coverage of reflectivity in the MDR data resulting in part from the coarse resolution of the MDR data brings too much moisture into the model. By comparing the MDR reflectivity and satellite imagery used at initialization time (Figs. 17 and 18), it is evident that MDR reflectivity covers areas where there are no clouds. MDR enhancement does provide better moisture distribution compared to the nested simulation run without any moisture enhancement. MDR enhancement improves the precipitation distribution on the active days but results in too much precipitation on the suppressed days.

The satellite imagery provides greater areal coverage than the MDR away from the land and does not have the resolution limitation of the MDR data. The main problem identified when enhancing the MASS relative humidity field with only satellite imagery is a tendency to underestimate moisture and precipitation. Because the algorithm in MASS allows the relative humidity field to be dried where no clouds are observed, relative humidity levels in the vicinity of any cloud that develops in the real atmosphere after initialization of the model

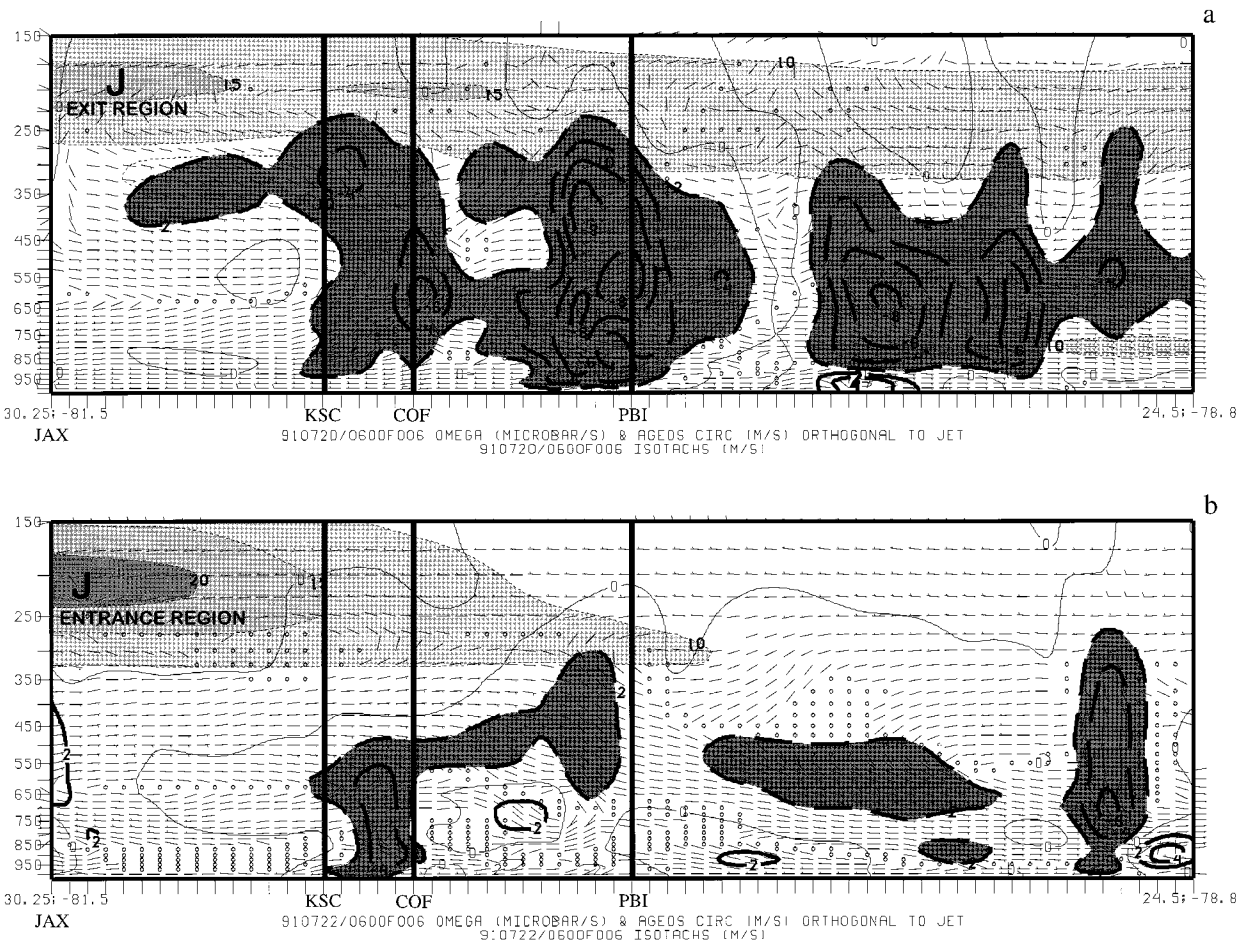

FIG. 16. As in Fig. 15 except for MASS 6-h nested grid forecasts for (a) 1200 UTC 20 July 1991 and (b) 1200 UTC 22 July 1991.

is likely to be underestimated in the simulation due to the drier model atmosphere; an important consideration with mesoscale convection due to the timescale of the phenomena. When only satellite data were used to enhance the model relative humidity on 20 July, the model atmosphere was significantly dried based on the lack of cloud at initialization time (Fig. 18b). The resultant relative humidity fields and precipitation generated by MASS were nearly as dry as 22 July.

Of the three types of derived moisture sources, the surface cloud observations had the least effect. As discussed previously, data from surface observations are incorporated indirectly into the model through a fairly complex scheme including a classification system, dataset comparison, and statistical prediction equations to interpolate the surface data to a collocated sounding. Examination of the relative humidity fields in both the 700-mb forecast and the vertical cross-sectional forecast show little difference from the basic run with no moisture enhancement. There are minor differences in relative humidity values (within 10%), but the placement of the relative maximum and minimum values are nearly identical.

Experience shows that moisture enhancement from all three derived sources combined at initialization time provides the best simulation results. The results from a simulation without moisture enhancement (*control run*) and a simulation with all three sources enhancing the relative humidity field at initialization (*enhanced run*) are contrasted for the most active (20 July) and most suppressed (22 July) days.

The MASS forecast of 700-mb relative humidity for 20 July from the enhanced run shows an increase in relative humidity over most of the grid domain when compared to the control run (Fig. 20). The patterns of relative humidity are similar in both runs, with a band of relative humidity $\geq$70% extending from northeast of KSC southwestward across Florida into the Gulf of Mexico. The relative humidity in the KSC vicinity and over southeast Florida is higher in the enhanced model run as a result of the MDR data that override drying of the model atmosphere through the satellite moisture algorithm. The depth of the moisture can be seen in a vertical cross section of relative humidity (Fig. 21). A comparison of the control run to the enhanced run on 20 July reveals deeper moisture in the control run, as a

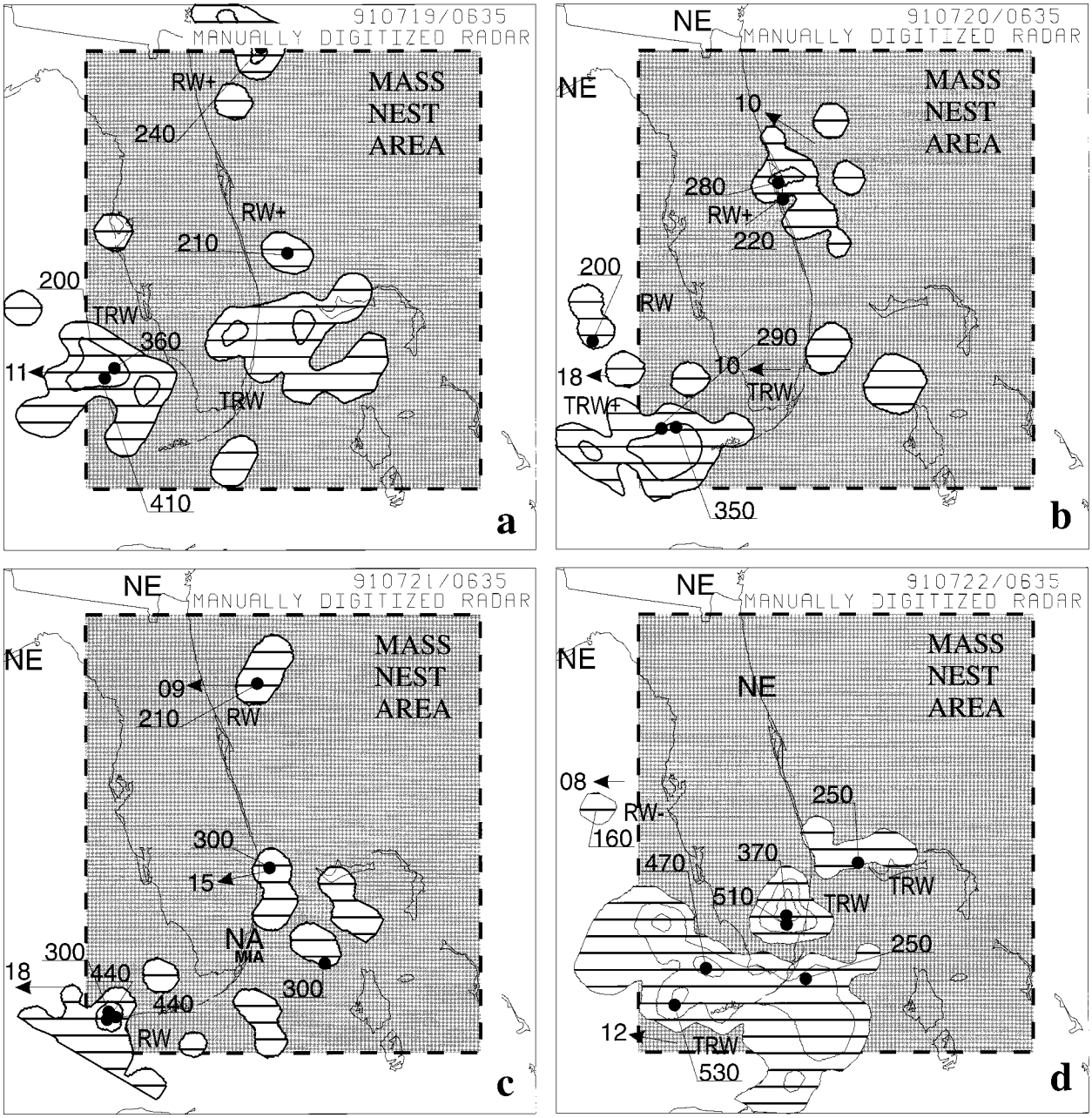

FIG. 17. Manually digitized radar (MDR) data with 40-km resolution used to enhance MASS nested run for (a) 0635 UTC 19 July 1991, (b) 0635 UTC 20 July 1991, (c) 0635 UTC 21 July 1991, and (d) 0635 UTC 22 July 1991. Nested grid domain is shaded lightly. MDR reflectivity echoes hatched and outlined. MDR reflectivity echoes, tops, and movement as shown in National Oceanic and Atmospheric Administration (1982).

result of drying of a portion of the model atmosphere by the satellite algorithm in the enhanced run. However, banded structure is observed in the relative humidity field in the enhanced run and not in the control run. The effect of the MDR enhancement is responsible for the appearance of the bands. Based on satellite imagery (see Fig. 2), the model atmosphere with the derived moisture sources performed better than the control run on 20 July.

The forecast patterns of relative humidity on 22 July (Fig. 21) for the control and enhanced runs are similar, but the enhanced run is more representative where the relative humidity is highest. One significant area of high relative humidity stretches from the Bahamas westward across south Florida and into the Gulf of Mexico. This area of moisture is associated with a large convective complex associated with a cold-core upper-tropospheric

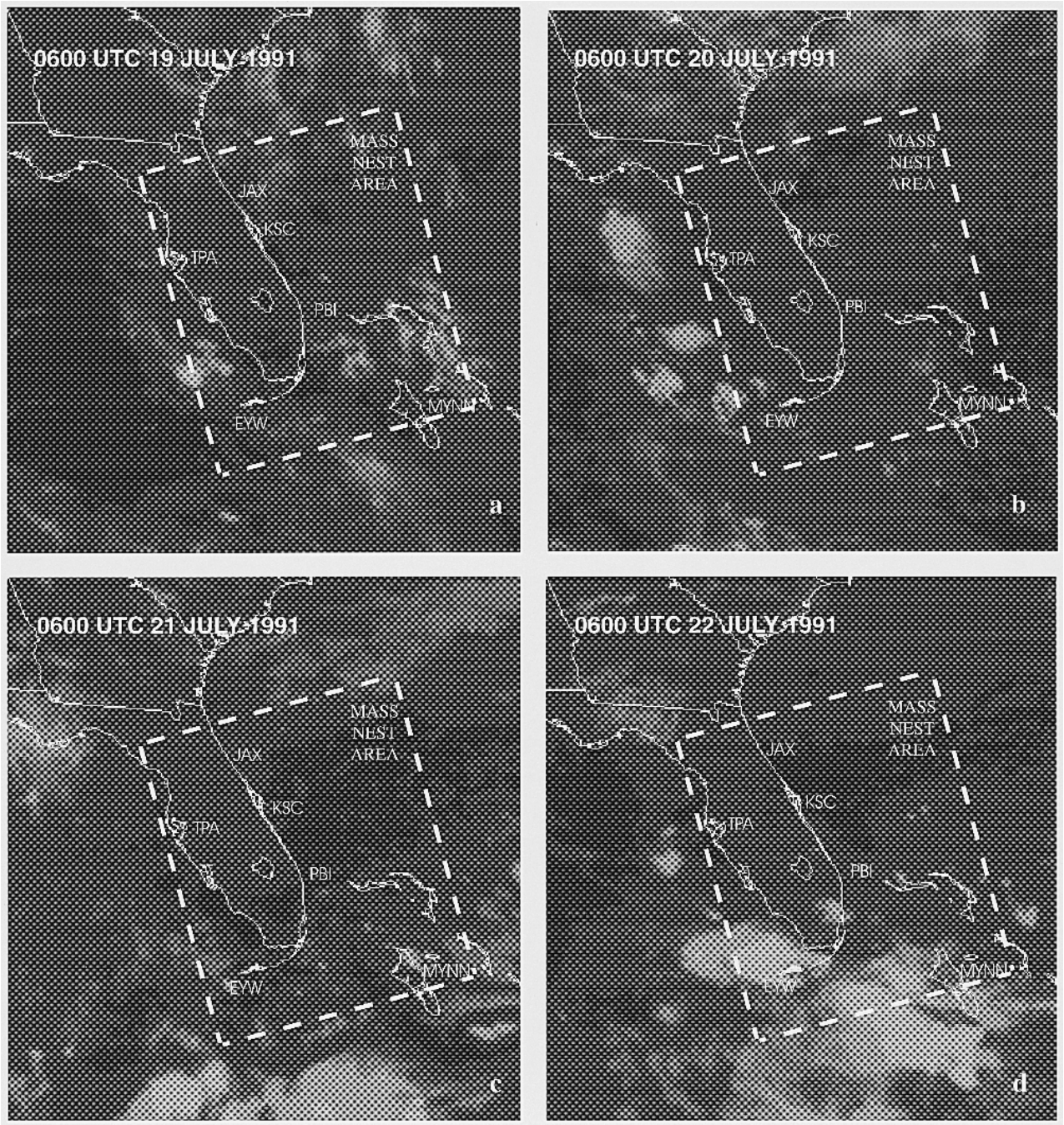

FIG. 18. *GOES-7* infrared satellite imagery with 4-km resolution used to enhance MASS nest run for (a) 0600 UTC 19 July 1991, (b) 0600 UTC 20 July 1991, (c) 0600 UTC 21 July 1991, and (d) 0600 UTC 22 July 1991. Nested grid domain is outlined in white-dashed box.

low. The control run underestimates relative humidity over this area by as much as 20%. Cross sections for 22 July (Fig. 22) show the moisture to be shallow and considerably drier than on 20 July. The enhanced run is drier in the KSC vicinity than the control run and it does a much better job simulating the moisture associated with the cold-core upper-tropospheric low seen at the southern end of the cross section than the control run when compared with IR satellite imagery (Fig. 23).

h. Model precipitation results

The precipitation fields generated in MASS come from the grid-scale moisture physics module using a

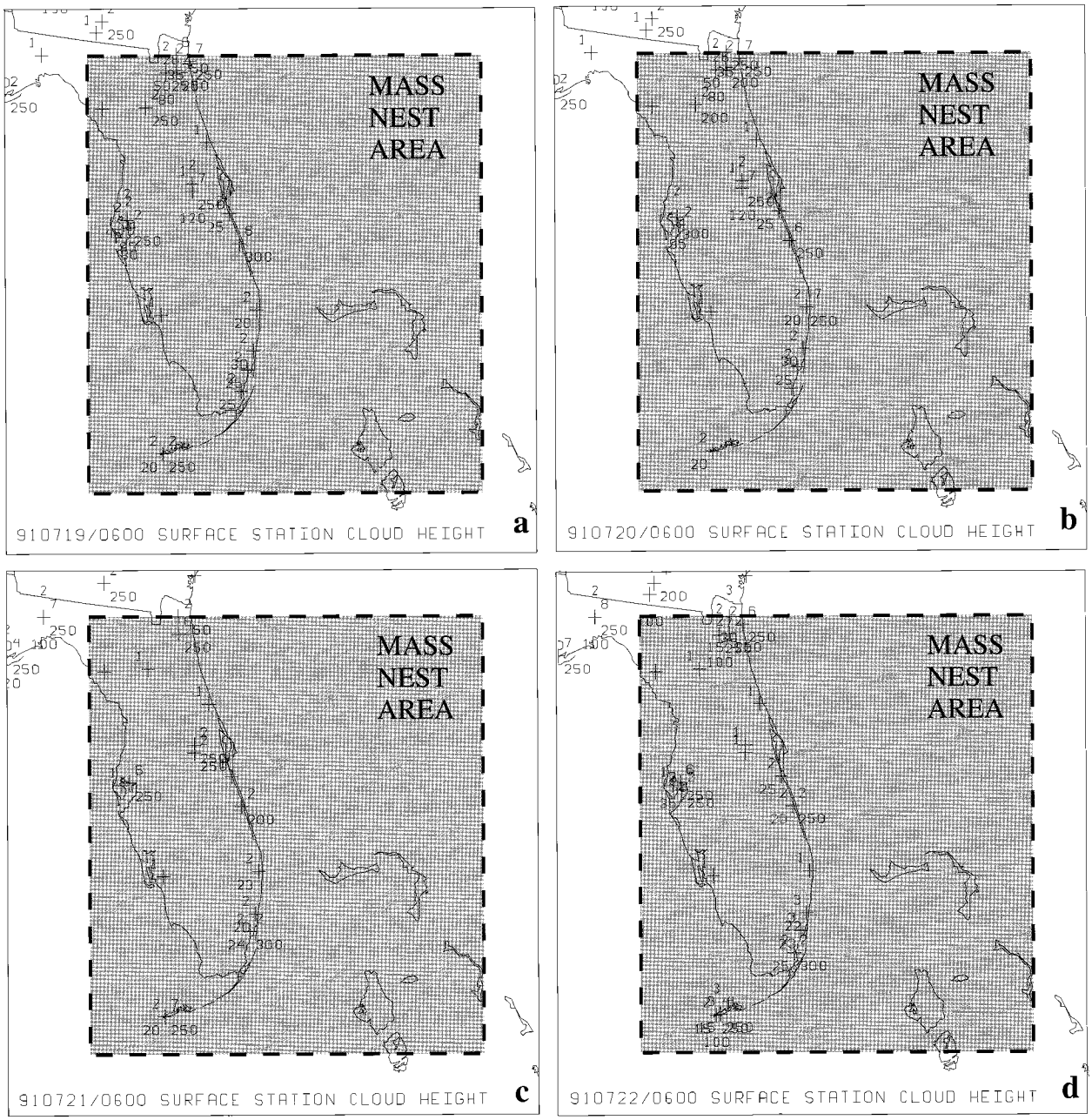

FIG. 19. Surface cloud observations used to enhance MASS nested run for (a) 0600 UTC 19 July 1991, (b) 0600 UTC 20 July 1991, (c) 0600 UTC 21 July 1991, and (d) 0600 UTC 22 July 1991. Nested grid domain is shaded lightly. Cloud observations are plotted as amount of low cloud in tenths to upper left of station and height of low cloud bases in hundreds of feet to lower left of station, amount of middle cloud in tenths above center of station and height of middle cloud bases in hundreds of feet below center of station, amount of high cloud in tenths to upper right of station and height of high cloud bases in hundreds of feet to lower right of station.

prognostic moisture scheme (MESO, Inc. 1995). By using the prognostic moisture scheme, conservation equations for cloud water, cloud ice (q_c), and rain-snow water (q_r) are added to the MASS basic set of prognostic equations. The precipitation fallout term is integrated from the top of the model atmosphere downward, and any condensate reaching the bottom of the model's lowest layer (the surface) is accumulated as precipitation.

Cumulative convective precipitation was totaled over 6 h ($\pm$3 h of 1200 UTC) on 20 and 22 July (Fig. 24). The patterns of precipitation produced by the control and enhanced simulations are similar, but the enhanced run generates more precipitation on both days. On 20 July the enhanced run shows an organized precipitation pattern in the form of two rainbands east and northeast of KSC and a band of precipitation along the east coast

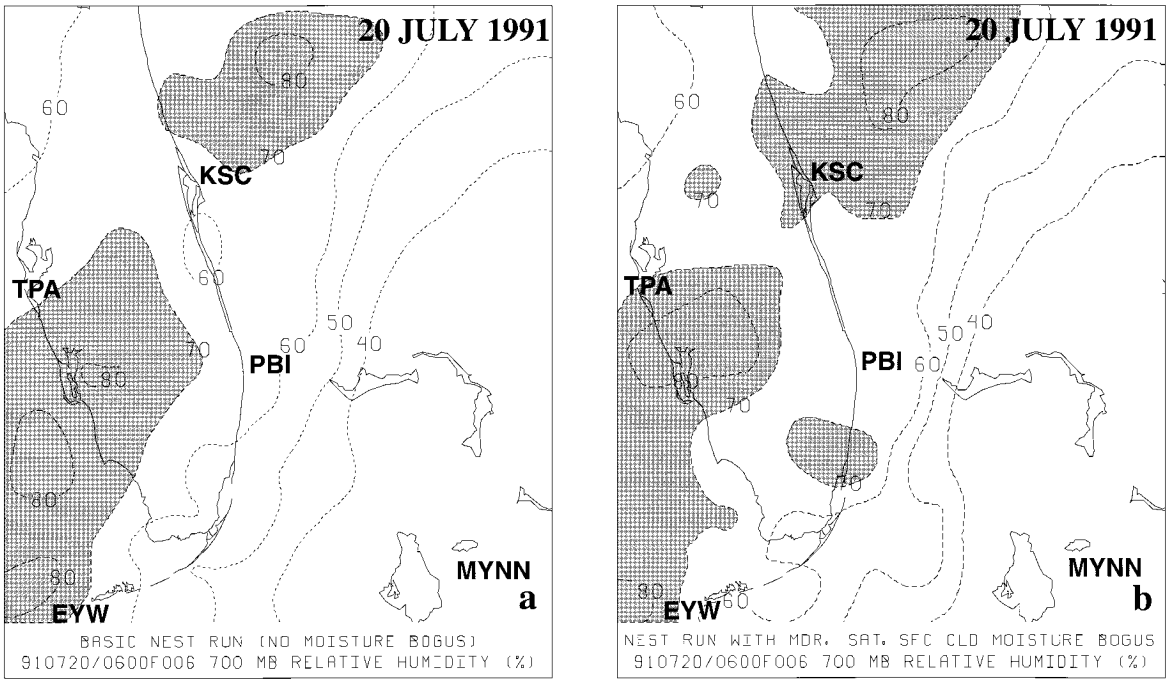

FIG. 20. MASS 6-h nested grid forecasts of 700-mb relative humidity (dashed contours every 10%, shaded above 70%) from the control run (no moisture enhancement) for (a) 1200 UTC 20 July 1991 and from the enhanced run (MDR, satellite, and surface cloud observation) for (b) 1200 UTC 20 July 1991.

of Florida (Fig. 24b). This pattern is not as well defined in the control run (Fig. 24a). MASS correctly simulated the large convective region northwest of EYW. The enhanced run produced 27 mm of precipitation over 6 h in the core of the convective complex northwest of EYW, whereas MDR indicated a maximum of VIP 5 with 49 000-ft echo tops between 0935 and 1335 UTC. The control run simulated only 18 mm of precipitation with this convective complex.

Although there were no clouds observed in the satellite imagery, nor any precipitation echoes on the MDR at initialization time on 22 July, MASS simulated a few small pockets of precipitation in the KSC vicinity (Fig. 24). The enhanced run produced more precipitation than the control run, yet there was no precipitation on this day. MASS did correctly simulate the precipitation occurring between southeast Florida and the Bahamas Islands associated with the 150-mb cold low. As in the simulation for 20 July, the enhanced run generated considerably more precipitation in the vicinity of this large convective complex than the control run.

5. Summary and conclusions

Experience has shown that short-term forecasting of convective activity in the vicinity of KSC during easterly (onshore) flow is a particularly challenging problem since the initiation of convection is generally not associated with sea-breeze and land-breeze activity. Seemingly similar synoptic regimes are present in cases that produce conditions ranging from clear skies to heavy showers. In addition, shower activity during easterly flow tends to form during morning hours when space shuttle launches are commonly scheduled.

Four days of onshore flow during the CaPE experiment were analyzed; two active, one passive, and one suppressed convective day at Kennedy Space Center. A careful regional analysis that included Global Optimal Interpolation data as a first-guess field and 20-m-height contouring at 150 mb uncovered distinctions between the 4 days. A subtropical jet streak at 150 mb developed in response to the northwestward movement of an upper-level cold-core low from the Bahamas over Florida. The propagation of the jet streak across Florida led to a shift from divergence to convergence aloft during the period 19 July to 22 July. The mid- to upper-tropospheric column mass adjustment over central Florida supported upper-level divergence with coupled low-level convergence on the convectively active days, 19 and 20 July, whereas on 21 and 22 July, convection was suppressed and the mid- to upper-level column mass adjustment was opposite that of the two active days, consistent with the conceptual model for jet streak dynamics (Uccellini and Johnson 1979). Rawinsonde observations, the regional analysis, and numerical simulations all support the suggestion that transverse circulations associated with the upper-tropospheric jet streak distinguish the active from passive days. The signature of subsidence drying in water vapor imagery was consistent with the observed wind maxima aloft and associated ageostroph-

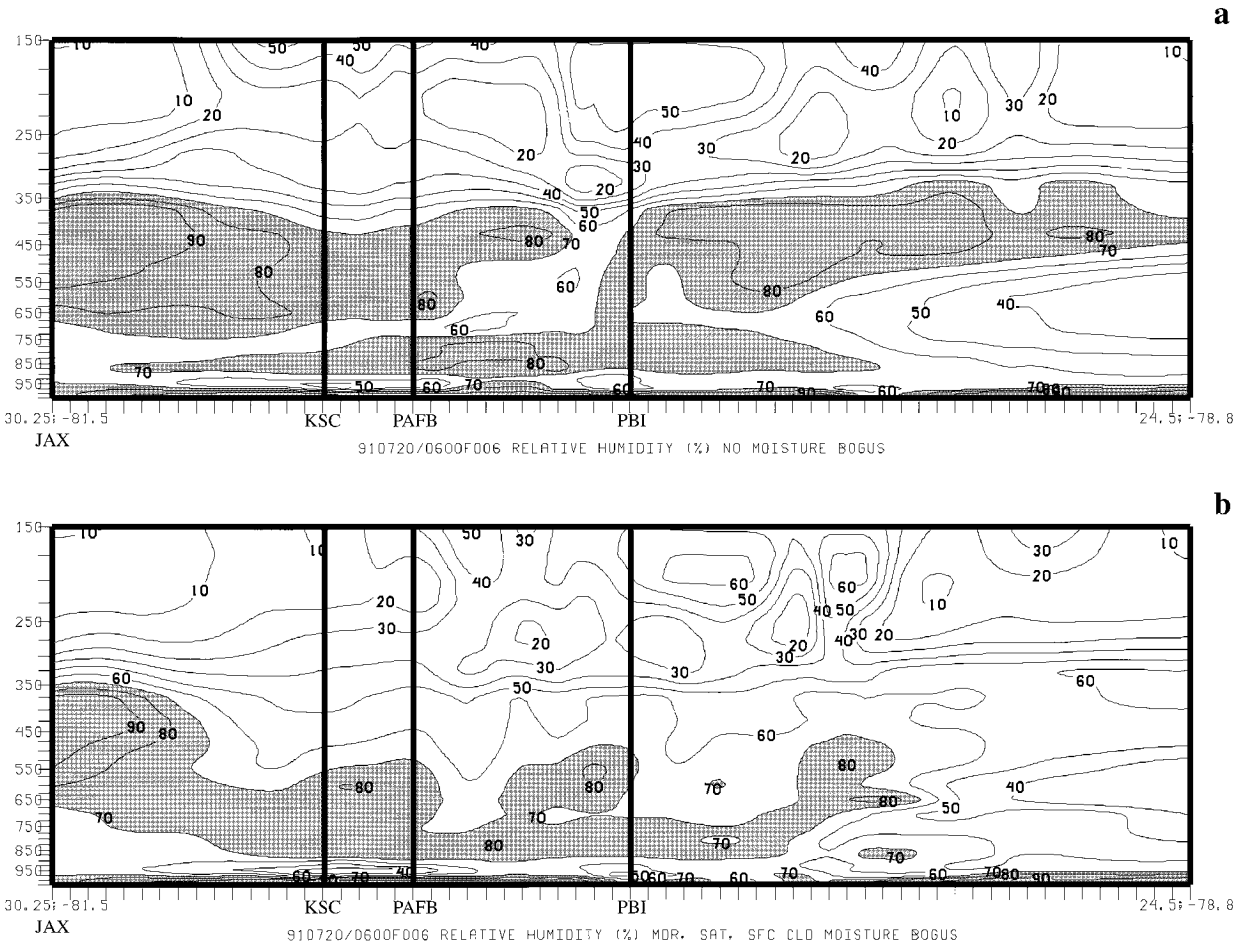

FIG. 21. Vertical cross sections of MASS 6-h nested grid forecasts of 700-mb relative humidity (solid contours every 10%, shaded above 70%) from the control run (no moisture enhancement) for (a) 1200 UTC 20 July 1991 and from the enhanced run (MDR, satellite, and surface cloud observation) for (b) 1200 UTC 20 July 1991. Cross sections were taken orthogonal to the 150-mb jet streak and convective rainbands (see Fig. 11 for location).

ic circulations. In conjunction with enhanced regional analysis and numerical model output, the high spatial and temporal resolution of the satellite observations represent a key resource for predicting the location and timing of convection during easterly flow regimes. We believe that the upper-level subtropical jet streak is a good feature for forecasters to monitor and apply to convection forecasts.

Analysis of sounding data showed elevated moisture above the marine boundary layer on convectively active days. Consequently, of all the stability indices, only the K index, which references 700-mb moisture, was found to have modest utility in discriminating convective activity in the vicinity of KSC. Given the critical importance of the water vapor distribution in forecasting convection, it is interesting to consider the addition of water vapor observations derived from the Global Positioning System (GPS) (Bevis et al. 1992; Businger et al. 1996). Ground-based GPS receivers can provide accurate integrated water vapor measurements every 30 min from the GPS signal delay introduced by water vapor overlying the receiver (Duan et al. 1996). GPS receivers placed at locations along the east coast of Florida, stationary buoys offshore, the Bahamas, Cuba, and the Dominican Republic could significantly improve the resolution of water vapor distribution during onshore flow. Many of these locations will have GPS receivers installed in the near term for purposes of navigation, and their data could be tapped for meteorological purposes (Kuo et al. 1993; Ware and Businger 1995).

Satellite data show shallow open-cell convection on all 4 days. On active days, convection was initiated at the apex of shallow open cells and subsequently organized into longitudinal rainbands seen in radar scans. The rainbands were oriented parallel to the cloud-layer wind shear and propagated with the mean wind in the cloud layer, consistent with the predictions of mixed mode wave-CISK in which buoyancy is the primary energy source maintaining the rainbands.

The MASS model was used to simulate the weather

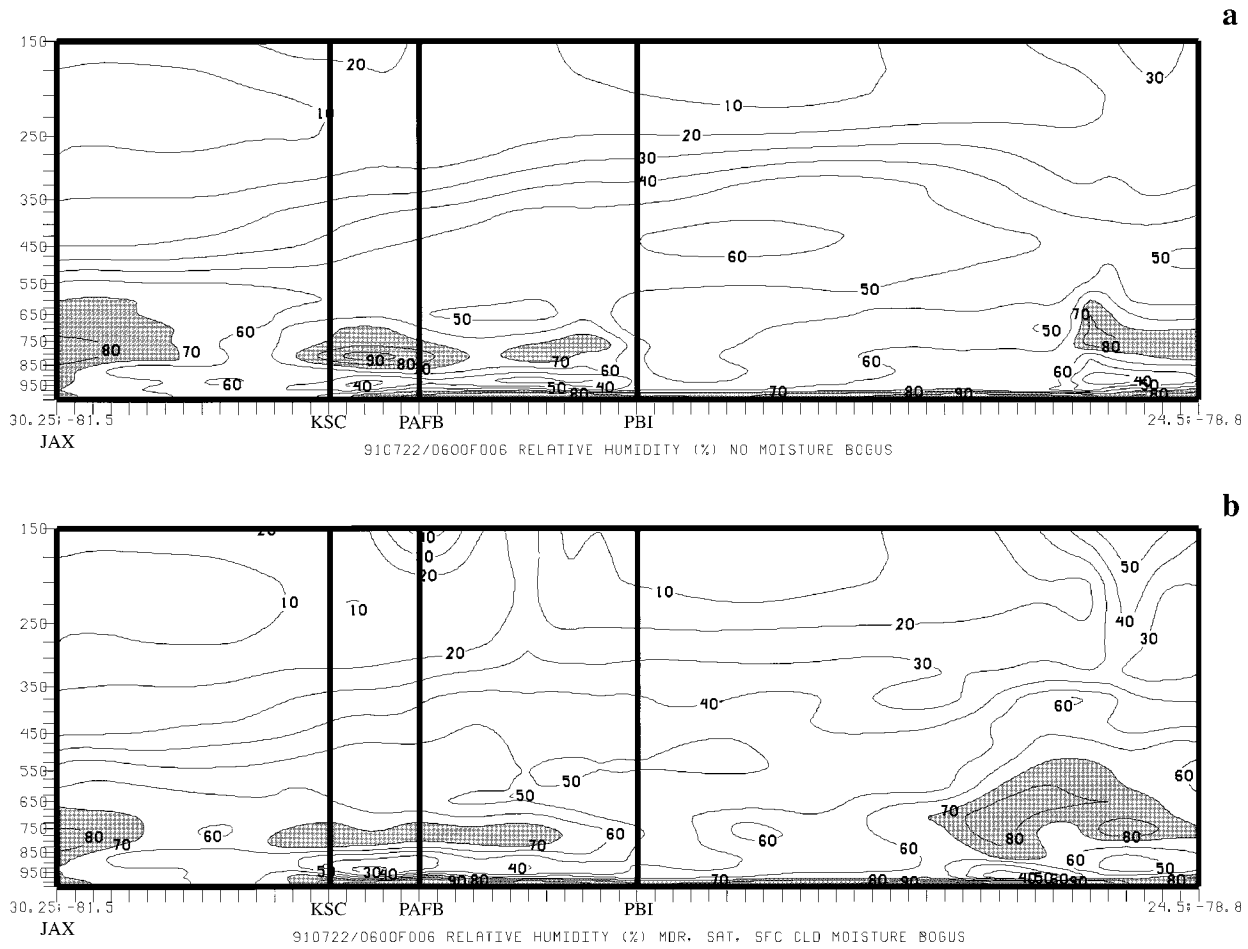

FIG. 22. As in Fig. 21 but for 22 July 1991.

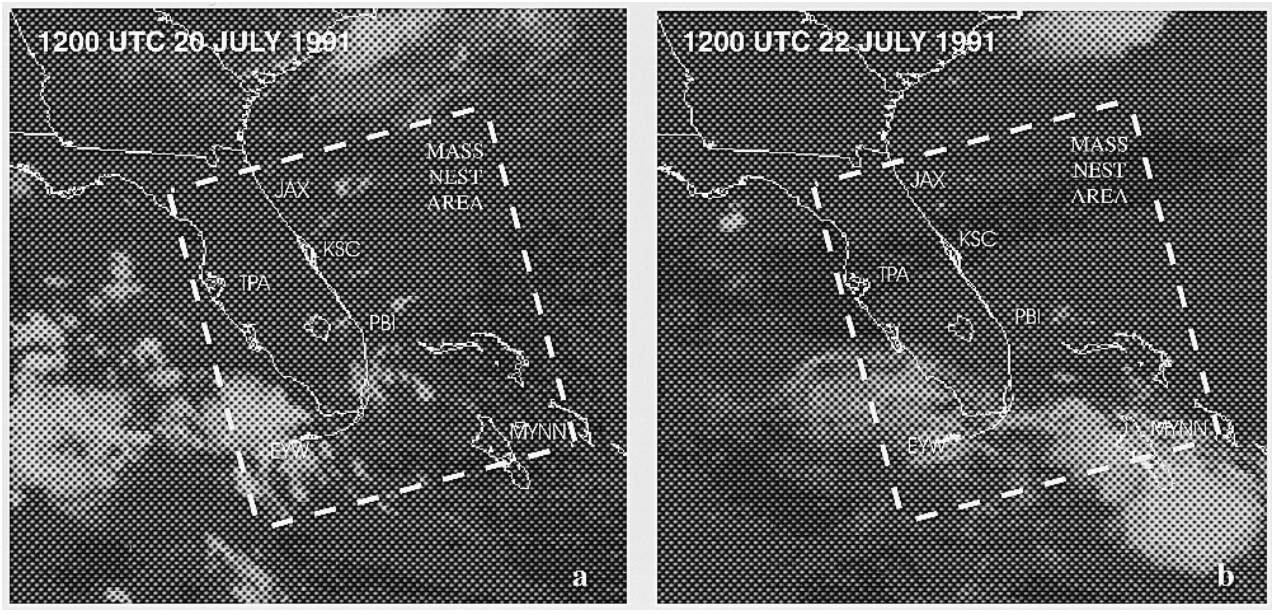

Fig. 23. Infrared satellite imagery (4-km horizontal resolution) from *GOES-7* for (a) 1431 UTC 19 July 1991, (b) 1431 UTC 20 July 1991, (c) 1431 UTC 21 July 1991, and (d) 1431 UTC 22 July 1991. Location of KSC indicated.

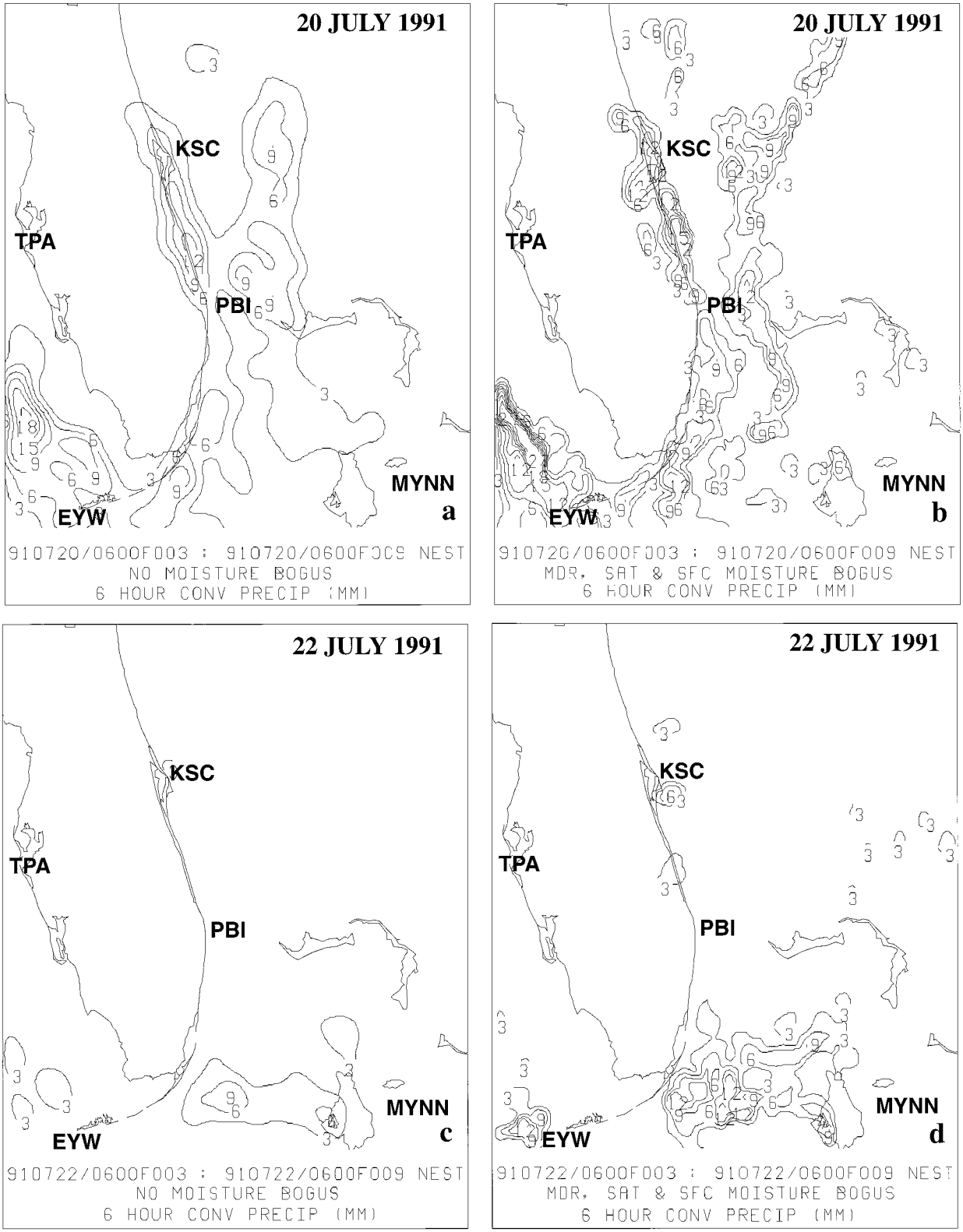

FIG. 24. MASS nested grid 3–9-h cumulative convective precipitation forecast (solid contours every 3 mm) from the control run (no moisture enhancement) for (a) 0900–1500 UTC 20 July 1991 and from the enhanced run (MDR, satellite, and surface cloud observation) for (b) 0900–1500 UTC 20 July 1991.

over the Florida peninsula and surroundings. To investigate the large-scale dynamics and provide initial conditions for a nested run, the model was initially run with a coarse (45 km) grid. The coarse run correctly simulated the movement of the cold low aloft, the development of the 150-mb jet streak, and attendant transverse ageostrophic circulations.

The MASS model run with a nested (11 km) grid successfully simulated mesoscale patterns of convective precipitation over the Florida peninsula and proximate coastal environment. Sensitivity studies were done by enhancing the initial model state with synthetic relative humidity derived from radar, satellite, and surface data. The best overall forecast patterns of precipitation and relative humidity resulted when the nested simulation included all derived moisture sources into the initial model state. Individually, the model results show that (i) manually digitized radar data increased the moisture in the model atmosphere each day, (ii) infrared satellite imagery increased the moisture in the model atmosphere when cloud was present but decreased the moisture and suppressed precipitation when cloud was not present, and (iii) enhancement of moisture from surface cloud observations produced little change in the forecast moisture distribution.

To make continued improvements in short-term forecasts of convective activity in support of the space program, ongoing research concerning the optimum employment of new data sources (*GOES-8*, WSR-88D Doppler radar, GPS data, etc.) is recommended. Also, a climatological study of easterly flow events in the vicinity of KSC would provide added value to this study, which was based on 4 days of data from CaPE. Operational meteorologists concerned with forecasting along the Florida east coast should test the hypotheses and findings of this work. Based on the results presented here, operational application of mesoscale numerical models with increasing resolution and enhanced data assimilation should result in tangible improvements in our ability to nowcast convective activity in the vicinity of KSC.

Acknowledgments. We would like to thank Steve Chiswell and Bob Rozumalski for significant computer support and help with data analysis. We appreciate the meteorological skill Tom Graziano has given to improve data analysis. Allen Riordan, Steve Koch, and Sethu Raman provided helpful suggestions to guide the research. We are most grateful to John Zack, Ken Waight, and everyone else at MESO, Inc., who provided the MASS model to us and answered all of our questions. Funding for this research was provided by the U.S. Air Force Air Weather Service through COMET Grants UCAR S9335 and UCAR S9341. This research is supported by the National Science Foundation under Grants ATM-9207111 and ATM-9496335.

REFERENCES

Adler, R. F., and A. J. Negri, 1988: A satellite infrared technique to estimate tropical convective and stratiform rainfall. *J. Appl. Meteor.,* **27,** 30–51.

Anderson, R., J. Gurka, and S. Steinmetz, 1982: Applications of VAS multispectral imagery to aviation forecasting. Preprints, *Ninth Conf. on Weather Forecasting and Analysis,* Seattle, WA, Amer. Meteor. Soc., 227–234.

Arritt, R. W., 1993: Effects of the large-scale flow on characteristic features of the sea breeze. *J. Appl. Meteor.,* **32,** 116–125.

Barnes, S. L., 1964: A technique for maximizing details in numerical weather map analysis. *J. Appl. Meteor.,* **3,** 396–409.

——, 1973: Mesoscale objective analysis using weighted time-series observations. NOAA Tech. Memo. ERL NSSL-62, Norman, OK, 60 pp. [Available from NOAA/ERL, 1313 Halley Circle Norman, OK 73069.]

Bauman, W. H., and S. Businger, 1996: Nowcasting for space shuttle landings at Kennedy Space Center, Florida. *Bull. Amer. Meteor. Soc.,* **77,** 2295–2305.

Bennetts, D. A., and B. J. Hoskins, 1979: Conditional symmetric instability—A possible explanation for frontal rainbands. *Quart. J. Roy. Meteor. Soc.,* **105,** 945–962.

Bevis, M., S. Businger, T. A. Herring, C. Rocken, R. A. Anthes, and R. H. Ware, 1992: GPS meteorology: Remote sensing of atmospheric water vapor using the Global Positioning System. *J. Geophys. Res.,* **97,** 15 787–15 801.

Blanchard, D. O., and R. E. López, 1985: Spatial patterns of convection in south Florida. *Mon. Wea. Rev.,* **113,** 1282–1299.

Boybeyi, Z., and S. Raman, 1992: A three-dimensional numerical sensitivity study of convection over the Florida peninsula. *Bound.-Layer Meteor.,* **60,** 325–359.

Burpee, R. W., 1979: Peninsula-scale convergence in the south Florida sea breeze. *Mon. Wea. Rev.,* **107,** 852–860.

Businger, S., and P. V. Hobbs, 1987: Mesoscale structure of two comma cloud systems over the Pacific Ocean. *Mon. Wea. Rev.,* **115,** 1908–1928.

——, and B. Walter, 1988: Comma cloud development and associated rapid cyclogenesis over the Gulf of Alaska: A case study using aircraft and operational data. *Mon. Wea. Rev.,* **116,** 1103–1123.

——, and Coauthors, 1996: The promise of GPS in atmospheric monitoring. *Bull. Amer. Meteor. Soc.,* **77,** 5–18.

Byers, H. R., and H. R. Rodebush, 1948: Causes of thunderstorms of the Florida peninsula. *J. Meteor.,* **5,** 275–280.

desJardins, M. L., K. F. Brill, S. Jacobs, S. S. Schotz, and P. Bruehl, 1992: *GEMPAK5 Users Manual Version 5.1.* NASA/GSFC, National Meteorological Center, and Unidata Program Center/UCAR, 267 pp.

Duan, J., and Coauthors, 1996: GPS meteorology: Direct estimation of the absolute value of precipitable water. *J. Appl. Meteor.,* **35,** 830–838.

Durran, D., and D. B. Webber, 1988: An investigation of the poleward edges of cirrus clouds associated with midlatitude jetstreams. *Mon. Wea. Rev.,* **116,** 702–714.

Emanuel, K. A., 1994: *Atmospheric Convection.* Oxford University Press, 580 pp.

Estoque, M. A., 1962: The sea breeze as a function of the prevailing synoptic situation. *J. Atmos. Sci.,* **19,** 24–25.

Fitzpatrick, P. J., J. A. Knaff, C. W. Landsea, and S. V. Finley, 1995: Documentation of a systematic bias in the aviation model's forecast of the Atlantic tropical upper-tropospheric trough: Implications for tropical cyclone forecasting. *Wea. Forecasting,* **10,** 433–446.

Foote, G. B., 1991: Scientific overview and operations plan for the convection and precipitation/electrification program. National Center for Atmospheric Research, Boulder, CO, 145 pp. [Available from NCAR, P.O. Box 3000, Boulder, CO 80307.]

Frank, N. L., P. L. Moore, and G. E. Ficher, 1967: Summer shower distribution of the Florida peninsula as deduced from digitized radar data. *J. Appl. Meteor.,* **6,** 309–316.

Hamill, T. M., R. P. D'Entremont, and J. T. Bunting, 1992: A description of the air force real-time nephanalysis model. *Wea. Forecasting,* **7,** 288–306.

Kaplan, M. L., J. W. Zack, V. C. Wong, and J. J. Tuccillo, 1982: Initial results from a mesoscale atmospheric simulation system and comparisons with the AVE-SESAME I data set. *Mon. Wea. Rev.,* **110,** 1564–1590.

Kocin, P. J., and L. W. Uccellini, 1990: *Snowstorms along the Northeastern Coast of the United States: 1955 to 1985. Meteor. Monogr.,* No. 44, Amer. Meteor. Soc., 280 pp.

Kuo, Y.-H., Y.-R. Guo, and E. R. Westwater, 1993: Assimilation of precipitable water measurements into mesoscale numerical models. *Mon. Wea. Rev.,* **121,** 1215–1238.

LeMone, M. A., 1973: The structure and dynamics of horizontal roll vortices in the planetary boundary layer. *J. Atmos. Sci.,* **30,** 1077–1091.

Lindzen, R. S., 1974: Wave-CISK in the tropics. *J. Atmos. Sci.,* **31,** 156–179.

Manobianco, J., J. W. Zack, and G. E. Taylor, 1996: Workstation-based real-time mesoscale modeling designed for weather support operations at the Kennedy Space Center and Cape Canaveral Air Station. *Bull. Amer. Meteor. Soc.,* **77,** 653–672.

MESO, Inc., 1995: *MASS Reference Manual Version 5.5.* MESO, 120 pp. [Available from MESO, Inc., 185 Jordon Road, Troy, NY 12180.]

National Oceanic and Atmospheric Administration, 1982: *National Weather Service Radar Code User's Guide, Federal Meteorological Handbook No. 7,* NOAA, 184 pp.

——, 1985: NCEP models and automated operations. NOAA Tech. Publ. Bulletin 355, NOAA, 11 pp. [Available from Program Requirements and Planning Division, NOAA, Silver Spring, MD 20910.]

Neumann, C. J., 1971: The thunderstorm forecasting system at the Kennedy Space Center. *J. Appl. Meteor.,* **10,** 921–936.

Parke, P. S., 1986: *Satellite Imagery Interpretation for Forecasters: Weather Service Forecasting Handbook No. 6.* NOAA, NESDIS, 610 pp.

Peppler, R. A., 1988: A review of static stability indices and related thermodynamic parameters. Illinois State Water Survey Misc. Publ. 104, 87 pp. [Available from Climate and Meteorology Section, Illinois State Water Survey, Champaign, IL 61820.]

Pielke, R., 1974: A three-dimensional numerical model of the sea breeze over south Florida. *Mon. Wea. Rev.,* **102,** 115–139.

——, 1975: Influence of the sea breeze on weather and man. *Weather,* **30,** 208–221.

Reap, R. M., 1994: Analysis and prediction of lightning strike distributions associated with synoptic map types over Florida. *Mon. Wea. Rev.,* **122,** 1698–1715.

Scofield, R. A., and J. F. W. Purdom, 1993: The use of satellite data for mesoscale analysis and forecasting applications. *Mesoscale Meteorology and Forecasting,* P. S. Ray, Ed., Amer. Meteor. Soc., 118–150.

Sun, W.-Y., 1978: Stability analysis of deep cloud streets. *J. Atmos. Sci.,* **35,** 466–483.

Uccellini, L. W., and D. R. Johnson, 1979: The coupling of upper and lower tropospheric jet streaks and implications for the development of severe convection. *Mon. Wea. Rev.,* **107,** 682–703.

Ware, R., and S. Businger, 1995: Global positioning for geosciences research. *Eos, Trans. Amer. Geophys. Union,* **76,** 187.

Watson, A. I., R. L. Holle, R. E. Lopez, R. Ortiz, and J. R. Nicholson, 1991: Surface wind convergence as a short-term predictor of cloud-to-ground lightning at Kennedy Space Center. *Wea. Forecasting,* **6,** 49–64.

Whitfield, M. B., and S. W. Lyons, 1992: An upper-tropospheric low over Texas during summer. *Wea. Forecasting,* **7,** 89–106.

Zack, J. W., V. M. Karyampudi, C. A. Mattocks, and G. D. Coats, 1988: Meso-beta scale simulations of convective cloud systems over Florida utilizing derived data derived from GOES satellite imagery. Preprints, *Eighth Conf. on Numerical Weather Prediction,* Baltimore, MD, Amer. Meteor. Soc., 293–300.

——, C. A. Mattocks, and M. D. Bousquet, 1991: A statistical-dynamical mesoscale thunderstorm forecast system for the Kennedy Space Center. Preprints, *Ninth Conf. on Numerical Weather Prediction,* Denver, CO, Amer. Meteor. Soc., 447–450.